Министерство образования и науки Российской Федерации
Федеральное государственное автономное образовательное учреждение
высшего профессионального образования
**«НАЦИОНАЛЬНЫЙ ИССЛЕДОВАТЕЛЬСКИЙ
ТОМСКИЙ ПОЛИТЕХНИЧЕСКИЙ УНИВЕРСИТЕТ»**

Институт – Энергетический институт
Направление (специальность) - 13.04.01 Теплоэнергетика и теплотехника
Кафедра атомных и тепловых электростанций

МАГИСТЕРСКАЯ ДИССЕРТАЦИЯ

Тема работы
Математическое моделирование конвективного тепломассопереноса вблизи вертикальной стенки, расположенной в наножидкости Mathematical simulation of convective heat and mass transfer of nanofluid near the vertical wall

УДК 536.25.532.5-022.532.519.876

Студент

Группа	ФИО	Подпись	Дата
5БМ5Б	Хоанг Конг Хиеп		

Руководитель

Должность	ФИО	Ученая степень, звание	Подпись	Дата
Профессор	М.А Шеремет	д. ф.-м. н, Доцент		

КОНСУЛЬТАНТЫ:

По разделу «Финансовый менеджмент, ресурсоэффективность и ресурсосбережение»

Должность	ФИО	Ученая степень, звание	Подпись	Дата
Доцент	Попова С.И	к. э. н, доцент		

По разделу «Социальная ответственность»

Должность	ФИО	Ученая степень, звание	Подпись	Дата
Доцент	Василевский М.В	к. т. н, доцент		

По нормоконтроль

Должность	ФИО	Ученая степень, звание	Подпись	Дата
Старший преподаватель	Вагнер Марина Анатольевна			

ДОПУСТИТЬ К ЗАЩИТЕ:

Заведующий кафедрой	ФИО	Ученая степень, звание	Подпись	Дата
Доцент	Матвеев А.С	к. т. н, доцент		

Томск – 2017 г.

ABSTRACT

The master thesis contains 84 pages, 37 figures, 20 tables and 33 references.

Key words: Nanofluids, Natural convection, Vertical flat plate, Single-phase model, Buongiorno's model, Full Navier–Stokes equations, Numerical method.

Steady state natural convection heat transfer from an isothermal vertical wall embedded in a water-based nanofluid is studied numerically using single-phase model (Tiwari and Das model) and double-phase model proposed by Buongiorno.

The Buongiorno's model takes into account two important slip mechanisms in nanofluids including Brownian motion and thermophoresis. The study is formulated in terms of the dimensionless stream function, temperature and nanoparticles volume fraction. The governing equations in the case of single-phase model and double-phase model were formulated using boundary layer approach and were transformed to the set of ordinary differential equations using similarity method. Numerical analysis of the ordinary differential equations with corresponding boundary conditions has been performed using an in-house computational code (Runge–Kutta method with shooting technique) and also using function BVP4C in Matlab system. In the case of full Navier–Stokes equations, simulation on the basis of a single-phase model has been conducted using also an in-house computational code in dimensionless stream function, vorticity and temperature. These partial differential equations with corresponding boundary equations have been solved by finite difference method of the second-order accuracy. Efforts have been focused on the effects of key parameters such as nanoparticles volume fraction, material of nanoparticles, shape of nanoparticles, Lewis number, buoyancy-ratio parameter, Brownian motion parameter and thermophoresis parameter on the velocity profile, temperature profile and profile of nanoparticles volume fraction. Reduced Nusselt number and skin friction number are presented. It is found that the solutions for velocity and temperature in the case of single-phase model is the same as the solutions in the case double-phase model at certain values of key parameters.

ACKNOWLEDGEMENT

I would like to thank my research advisor, Dr. Mikhail Sheremet, for his continual instructions and interest in my studies and research work. Under his supervision, I have learned so much during the time of my master course. I also acknowledge the support of faculties working at department of Nuclear and Thermal Power Plants at Tomsk Polytechnic University. Finally, I would also like to thank my family and my friends, who supported me during my studies as a graduate student.

TABLE OF CONTENTS

List of Abbreviations

ISI – International Scientific Indexing

MWNTs – Multiwalled of carbon nanotubes

Wt% - Weight-weight percentage

Re – Reynolds number

CHF – Critical Heat Flux

nf – nanofluid

f – base fluid

Gr_x – local Grashof number

Cp – Specific heat capacity

D_B – Brownian diffusion coefficient

D_T – Thermal diffusion coefficient

Le – Lewis number

ODE – Ordinary differential equation

PDE – Partial differential equation

Pr – Prandtl number

Nb – Brownian motion parameter

Nt – thermophoresis parameter

Nr – buoyancy-ratio parameter

FDM – Finite Difference Method

1. INTRODUCTION

Starting in the 1980's, we have gradually become familiar with nanotechnology. Definitions, phrases about nanotechnology are no longer strange with human life, obviously, nanotechnology is changing the life around us thanks to human's influence on nanoscale. In this size, nano-materials show lots of promising properties. Thanks to potential users resulted from their properties, nanoparticles have been in the focus of many researchers. We can find out common applications such as: biomedicine, magnetic resonance imaging, data storage, environment remediation, heat transfer enhancement, etc. In recent years, one of nano-materials, which has attracted considerable attention, is nanofluid. Nanofluid is a suspension of nanoparticles in a base "conventional" fluid such as water, oil, ethylene glycols. The nanoparticles can be made of metals, oxides or carbon nanotubes. Nanofluids perform enhanced thermal conductivity and convective heat transfer coefficient as compared to the clear fluids. This new material provides an expectation that the present level of cooling technology can be improved significantly by creating fluids that are more conducting. Nanofluids were found to be very stable due to the small size of the particles and the small volume fraction of the particles needed for heat transfer enhancement. The discovery of nanofluid brought to our world a new brand of research including not only theoretical but also experimental works. Several thousands of publications in well-known journals have been carried out by researchers for nearly twenty years. In Fig. 1 we can see the exponentially increasing number of publications concerning nanofluids from Journal published in Web of Science data base. More attention to nanofluids can also be seen in the number of research groups in the most prestigious institutions worldwide such as Massachusetts Institute of Technology (MIT) and Royal Institute of Technology (Sweden). Moreover, research groups concerning nanofluids are being established in different industries such as electronic devices, heat exchangers, biomedicine. Nanofluid technology will thus be an emerging and exciting technology of the twenty-first century. With the continued miniaturization of technologies in many fields, nanofluids with a

capability of cooling high heat fluxes would be extremely important in the advancement of all high technology.

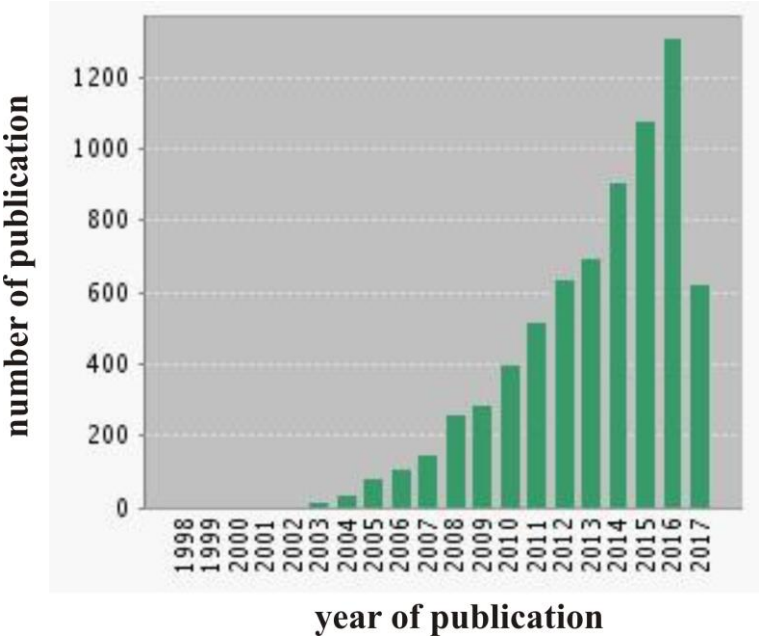

Fig. 1. *Annual number of publications in ISI journals from Web of Science database*

The concept of nanofluids originated from the higher thermal conductivity of metals in solid form as compared to thermal conductivity of traditional heat transfer fluids such as water, ethylene glycol, engine oils. As a result, investigators go to a new idea that the thermal conductivities of conventional heat transfer fluids could be significantly increased by dispersing nanoparticles with high thermal conductivities to the base fluids. The thermal conductivities of different materials at room temperature (25 ^{o}C) are shown in Table 1.

Table 1. Thermal conductivity at 25 ^{o}C of various materials

Material	**Thermal Conductivity (W/m·K)**
Air	0.024
Aluminum	205
Aluminum Oxide	30

Copper	401
Diamond	1000
Engine Oil	0.15
Ethylene Glycol	0.25
Water	0.613
Carbon Nanotubes	3000
Iron	80
Iron Oxide	0.58
Silver	429

Nanofluids come to our world and address two problems of conventional approach: the rapid settling of millimeter or micrometer-sized particles in fluids and the low conductivities of suspensions with low particle concentrations. In addition, such kind of nanofluids can help to avoid clogging in very small devices. In 1995, being aware of the superior properties of nanoparticles, Stephen U.S. Choi, who is a member of American Society of Mechanical Engineers, proposed an idea of dispersing nanometer-sized particles with typical length scales from 1 to 100 nm in base fluids. The obtained fluids in his research exhibited a heat transfer coefficient of two times higher than traditional fluids. The much greater thermal conductivity of nanofluids can be explained by the higher surface/volume ratio of nanoparticles, because heat transfer appears mainly on the surface of particles. We can also adjust the thermal conductivity and suspension stability of nanoparticles by changing their sizes.

There are two ways to produce nanofluids: one-step and two-step production methods. The two-step method first makes nanoparticles and then disperses them in host fluids. In the one-step method, we have to make and disperse nanoparticles into base fluids simultaneously.

The two-step technique is applied for nanofluids containing oxide nanoparticles and carbon nanotubes. Nanofluids manufactured by two-step method have to face some disadvantages: individual particles quickly agglomerate before

dispersion, and the settling of nanoparticle agglomerates in the liquids. As a result of poor quality of dispersion, the significantly enhanced thermal conductivity can not be achieved.

The one-step method can be divided into physical method and chemical method. The physical method can be used for creating non-agglomerating nanoparticles by condensing nano-phase powder from the vapor phase directly into a flowing low-vapor-pressure fluid. This physical method can produce stable and well-dispersed nanofluids with a great enhancement of thermal conductivity. The one-step chemical method developed by Zhu et al. [1] is faster and cheaper than physical method.

1.1. Experimental works

Many experimental works have discovered some distinctive features of nanofluids such as strong temperature-dependent thermal conductivity, strong size-dependent thermal conductivity. It can be found in some experiments on nanofluids that the laminar convection heat transfer coefficient increases by two times and critical heat flux increases by three times. Those superior properties of nanofluids can promise a revolution in heat removal technology. Copper nanofluid in the experiment by Eastman et al. [2] showed a 40% increase in the thermal conductivity at the volume fraction of only 0.3%. This experiment has demonstrated that metallic nanofluids with much lower concentration can be stable and possess much higher conductivity than nanofluids of oxides. Various other researches confirmed the non-linear relationship between thermal conductivity and concentration. Multi-Walled Carbon Nanotubes (MWCNTs) nanofluid in the experiment by Choi et al. [3] showed a 150% increases in the conductivity with only 1 vol% nanotubes. This experimental result is in contrast to theoretical predictions which exhibited a linear relationship. Hong et al. [4] also discovered the nonlinear relationship in the case of Fe-ethylene glycol nanofluids. It has been found that the $Al_{70}Cu_{30}$ nanofluids in the experimental work by Chopkar et al. [5] possess 200% enhancement in thermal conductivity at 2.0 vol% $Al_{70}Cu_{30}$ particles.

Das et al. [6] claimed that the temperature-dependent conductivity of nanofluids is much stronger than conventional fluids. In this experiment on Al_2O_3 and CuO water-based nanofluids, the thermal conductivity increases by 2 to 4 times with temperature change between 20 to 50 ^oC. In addition, the strongly size-dependent thermal conductivity of nanofluids is confirmed in the discovery by Chon et al. [7]. One year later, Chopkar et al. [5] measured the effect of particle size on the thermal conductivity of $Al_{70}Cu_{30}$ ethylene glycol-based nanofluids.

Nanofluids have been found to possess not only enhanced thermal conductivity but also better convective heat transfer coefficients. The laminar heat transfer coefficient can increase by 2 to 3.5 times for nanofluids. In 2004, Ding and Wen [8] studied a nanofluid containing 0.5 wt% of carbon nanotubes and they discovered that the convection heat transfer coefficient enhanced by 350% at Re = 800. Moreover, Xuan and Li [9] also showed their results in the significant increase of turbulent heat transfer coefficient of nanofluids. However, we see a different picture in the case of natural convection heat transfer coefficient. A study on natural convection of nanofluids was performed for the first time by Putra et al. [10]. This experiment performed that the decrease in natural convection heat transfer coefficient increases with concentration of nanoparticles.

Many researchers have studied boiling heat transfer in nanofluids. Some researchers claimed out the deterioration of pool boiling in nanofluids, but others also showed their results with increase of boiling heat transfer coefficient. In the case of critical heat flux (CHF), all investigators come to a conclusion that nanofluids possess the enhancement of CHF. This enhancement in CHF promises applications in many different industries such as reactors, lasers.

1.2. Theoretical works

Conventional models for heat conduction, convection, or boiling can not explain thermal properties of nanofluids. Therefore, a lot of studies are focusing on new physical concepts, mechanisms and new models for the enhanced thermal conductivity, critical heat flux, and the convection heat transfer coefficient of

nanofluids. Wang et al. [11] for the first time explained the enhanced thermal transport in nanofluids by particle motion, surface action and suggested the size-dependent thermal conductivity of nanofluids. Xuan and Li [12] introduced the increased surface area of nanoparticles, particle-particle collisions, the dispersion of nanoparticles. Keblinski et al. [13] recommended four microscopic mechanisms for the significantly increasing of thermal transport of nanofluids including: Brownian motion of the particles, molecular-level layering of the liquid at the liquid-particle interface, the ballistic rather than diffusive nature of heat conduction in the nanoparticles, and the effects of nanoparticle clustering. Yu and Choi [14] developed a renovated Maxwell model for the effective thermal conductivity of solid-liquid suspensions and then they renovated Hamilton-Crosser model. However, these models can not explain the nonlinear behavior of nanofluid thermal conductivity. On the basis of liquid layering mechanism and the average polarization theory, Xue [15] introduced a structure model, which was able to predict the nonlinear behavior of nanofluid thermal conductivity. Xie et al. [16] suggested the effect of the shape (spherical and cylindrical) of nanoparticles on enhancement of nanofluid thermal conductivity. The strongly pH-dependent thermal conductivity was reported by Lee et al. [17]. Yu and Choi [14] were first to suggest the nonlinear dependence on the particle-volume fraction of the thermal conductivity of nanofluids containing spherical nanoparticles.

Most of dynamic models consider nanoparticle motion as the main reason for enhanced thermal transport in nanofluids. Nanoparticle motion is also the reason for the strongly temperature-dependent thermal conductivity of nanofluids. A lot of investigators studied Brownian motion of nanofluids and they tend to conclude that Brownian movement of nanoparticles is primarily responsible for the enhanced thermal conductivity of nanofluids.

The significant enhancement of convective heat transfer of nanofluids as compared to base fluids has inspired some researchers to propose new models of enhanced convection heat transfer coefficient under both laminar and turbulent flow. Xuan and Li [12], Xuan and Roetzel [18], Khaled and Vafai [19] suggested

models, which considered thermal dispersion as a possible explanation for enhanced convection heat transfer in nanofluids. Buongiorno [20] studied seven mechanisms during the convection of nanofluids and reported that Brownian motion and thermophoresis are the most important mechanisms in laminar flow and in the viscous sub-layer of turbulent flow, but are negligible in the turbulent region. Kim et al. [21] analyzed the Soret effects on heat transfer of nanofluids. Theoretical works are continuing to be necessary for accurate models of nanofluids. Mechanisms and models may not be perfect, but we will move it closer to reality by developing our models step by step every day.

Thermal properties of nanofluids and their stability are very promising for applications such as biomedicine, cancer treatment, microelectronics cooling, but there are still technical barriers we have to face before achieving cost-effective, high-volume production of nanofluids. In the two-step method, nanofluids can be produced at low prices, but there are still some issues like aggregates and high-volume fraction needed for thermal conductivity enhancement. Investigators have proposed some innovative ways to improve the two-step method. The one-step method can produce well-dispersed nanofluids but it can provide only small quantities of nanofluids in laboratories. Therefore, researchers are trying to improve the one-step methods and scale up to commercial production.

Nanofluids are desirable for efficient use of energy in general or cooling technology in particular. However, some nanofluids can have negative impacts on environment and health. Therefore, it is vital for engineers and scientist to develop green nanofluids by choosing environment-friendly nanoparticles; for example: biodegradabe nanoparticles in biomedicine applications.

In this thesis work, we investigate the natural convection of nanofluid from an isothermal vertical flat plate using numerical method. Both single phase model and double phase models have been used for mathematical simulation and then a comparison between two models is carried out for the first time ever. In the present research, the full Navier-Stokes equations for the problem were also solved by using finite different method. Natural convection flows have various engineering

and industrial applications such as geothermal systems, heat exchangers, computer chips, nuclear waste, chemical reactors.

2. MATHEMATICAL MODEL

In the present chapter we will formulate a boundary-value problem for free convection of nanofluid from the vertical isothermal flat plate presented in Fig. 2.

It is assumed that an isothermal vertical plate is located within a nanofluid. Initial temperature of nanofluid T_∞ is less then the plate temperature T_w. Therefore, due to the temperature difference one can find a formation of convective flow in the form of ascending flow near the plate.

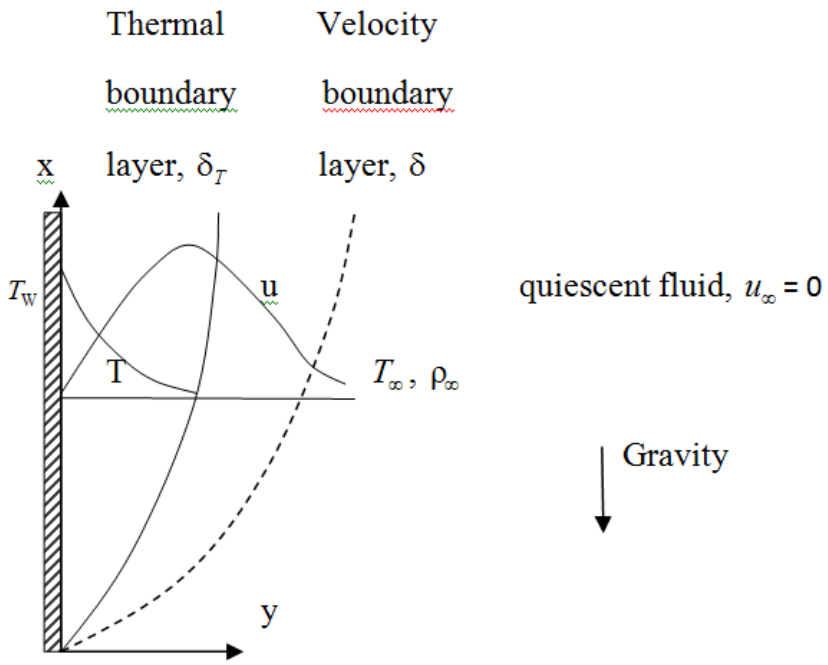

Fig. 2. *Physical model*

For mathematical description of this phenomenon we will use two models such as a single-phase model and double-phase model (Buongiorno model). Firstly, these models will be formulated in boundary-layer approach and solved using similarity technique. After that full Navier–Stokes equations will be solved in the case of isothermal vertical plate in an open cavity. Obtained models will be compared as a final analysis.

2.1. Boundary-layer approach

2.1.1. Single-phase model

For mathematical analysis we utilized partial differential equations on the basis of the boundary-layer approach taking into account the domain of ineterst presented in Fig. 1. These equations have been formulated using the conservation laws for mass, momentum and energy [22–24]:

$$\frac{\partial u}{\partial x}+\frac{\partial v}{\partial y}=0 \tag{1}$$

$$u\frac{\partial u}{\partial x}+v\frac{\partial u}{\partial y}=\frac{1}{\rho_{nf}}\left[\mu_{nf}\frac{\partial^2 u}{\partial y^2}+(\rho\beta)_{nf}\,g(T-T_\infty)\right] \tag{2}$$

$$u\frac{\partial T}{\partial x}+v\frac{\partial T}{\partial y}=\frac{1}{\left(\rho C_p\right)_{nf}}k_{nf}\frac{\partial^2 T}{\partial y^2} \tag{3}$$

The following boundary conditions have been added to the formulated governing equations:

$y=0:\ u=v=0,\ T=T_w;$

$y\to\infty:\ u\to 0,\ T\to T_\infty$

where T_w is the temperature of vertical wall and T_∞ is the temperature of ambient fluid.

For solution to the formulated boundary-value problem the author has used the similarity method with the following non-dimensional variables [22, 23]:

$$\eta=\frac{y}{x}\left(\frac{Gr_x}{4}\right)^{1/4},\ \psi=4\nu f(\eta)\left(\frac{Gr_x}{4}\right)^{1/4},\ \theta=\frac{T-T_\infty}{T_w-T_\infty},$$

where $Gr_x=\dfrac{g\beta x^3\left(T_w-T_\infty\right)}{\nu^2}$

Taking into account these new variables we can recalculate the velocity components:

$$u = \frac{\partial \psi}{\partial y} = 4\nu\left(\frac{Gr_x}{4}\right)^{1/4}\frac{\partial f}{\partial y} = 4\nu\left(\frac{Gr_x}{4}\right)^{1/4}\frac{\partial f}{\partial \eta}\frac{\partial \eta}{\partial y} = \frac{4\nu}{x}\left(\frac{Gr_x}{4}\right)^{1/2} f'$$

$$v = -\frac{\partial \psi}{\partial x} = -\frac{\partial}{\partial x}\left[4\nu f(\eta)\left(\frac{Gr_x}{4}\right)^{1/4}\right] = -\frac{\nu}{x}\left(\frac{Gr_x}{4}\right)^{1/4}(-f'\eta + 3f)$$

Then we can obtain derivatives of velocities and temperature as following:

$$\frac{\partial u}{\partial x} = \frac{\partial^2 \psi}{\partial x \partial y} = \frac{\partial}{\partial x}\left[\frac{4\nu}{x}\left(\frac{Gr_x}{4}\right)^{1/2} f'\right] = \frac{\nu}{x^2}\left(\frac{Gr_x}{4}\right)^{1/2}(2f' - f''\eta),$$

$$\frac{\partial u}{\partial y} = \frac{\partial^2 \psi}{\partial y^2} = \frac{\partial}{\partial y}\left[\frac{4\nu}{x}\left(\frac{Gr_x}{4}\right)^{1/2} f'\right] = \frac{4\nu}{x^2}\left(\frac{Gr_x}{4}\right)^{3/4} f'',$$

$$\frac{\partial^2 u}{\partial y^2} = \frac{\partial^3 \psi}{\partial y^3} = \frac{\nu Gr_x}{x^3} f''',$$

$$T - T_\infty = \theta(T_w - T_\infty),$$

$$\frac{\partial T}{\partial x} = \frac{\partial \theta}{\partial x}(T_w - T_\infty),$$

$$\frac{\partial T}{\partial y} = \frac{\partial \theta}{\partial y}(T_w - T_\infty),$$

$$\frac{\partial^2 T}{\partial y^2} = \frac{\partial^2 \theta}{\partial y^2}(T_w - T_\infty)$$

Velocities and temperature in Eqs. (1)–(3) can be replaced by non-dimensional variables then we get:

Eq. (2) can be written as follows:

$$\frac{\nu^2 Gr_x}{x^3}\left(2(f')^2 - \eta f' f''\right) - \frac{\nu^2 Gr_x}{x^3}\left(3ff'' - \eta f' f''\right) = \frac{\mu_{nf}}{\rho_{nf}}\frac{\nu Gr_x}{x^3} f''' +$$

$$+\frac{1}{\rho_{nf}}(\rho\beta)_{nf}\, g\theta(T_w - T_\infty)$$

$$\Leftrightarrow \frac{\nu^2 Gr_x}{x^3}(2(f')^2 - 3ff'') = \frac{\mu_{nf}}{\rho_{nf}}\frac{\nu Gr_x}{x^3} f''' + \frac{(\rho\beta)_{nf}}{\rho_{nf}\beta_f}\frac{\nu^2 Gr_x}{x^3}\theta$$

$$\Leftrightarrow \upsilon\left(2(f')^2 - 3ff''\right) = \upsilon_{nf} f''' + \frac{(\rho\beta)_{nf}}{\rho_{nf}\beta_f}\upsilon\theta$$

$$\Leftrightarrow \frac{\upsilon_{nf}}{\upsilon} f''' + 3ff'' - 2(f')^2 + \frac{(\rho\beta)_{nf}}{\rho_{nf}\beta_f}\theta = 0.$$

Eq. (3) can be written as follows:

$$\frac{4\nu}{x}\left(\frac{Gr_x}{4}\right)^{1/2} f'\frac{\partial\theta}{\partial x}(T_w-T_\infty)-\frac{\nu}{x}\left(\frac{Gr_x}{4}\right)^{1/4}(-f'\eta+3f)\frac{\partial\theta}{\partial y}(T_w-T_\infty)=$$

$$=\frac{1}{(\rho C_p)_{nf}}k_{nf}\frac{\partial^2\theta}{\partial y^2}(T_w-T_\infty)$$

$$\Leftrightarrow\frac{4\nu}{x}\left(\frac{Gr_x}{4}\right)^{1/2} f'\frac{\partial\theta}{\partial\eta}\frac{\partial\eta}{\partial x}(T_w-T_\infty)-\frac{\nu}{x}\left(\frac{Gr_x}{4}\right)^{1/4}(-f'\eta+3f)\frac{\partial\theta}{\partial\eta}\frac{\partial\eta}{\partial y}(T_w-T_\infty)=$$

$$=\frac{1}{(\rho C_p)_{nf}}k_{nf}\frac{\partial}{\partial y}\left[\frac{\partial\theta}{\partial\eta}\frac{\partial\eta}{\partial y}(T_w-T_\infty)\right]$$

$$\Leftrightarrow\frac{-\nu}{x^2}\left(\frac{Gr_x}{4}\right)^{1/2} f'\theta'\eta-\frac{\nu}{x^2}\left(\frac{Gr_x}{4}\right)^{1/2}(3f\theta'-\eta f'\theta')=\frac{k_{nf}}{\rho_{nf}Cp_{nf}}\frac{1}{x^2}\left(\frac{Gr_x}{4}\right)^{1/2}\theta''$$

$$\Leftrightarrow 3f\theta'+\frac{k_{nf}}{Cp_{nf}\mu_{nf}}\theta''=0$$

After taking into account the dimensionless variables, the governing equations can be written as a system of two ordinary differential equations:

$$\begin{cases}\dfrac{\mu_{nf}}{\rho_{nf}}\dfrac{\rho_f}{\mu_f}f'''+3ff''-2(f')^2+\dfrac{(\rho\beta)_{nf}}{\rho_{nf}\beta_f}\theta=0\\ 3f\theta'+\dfrac{k_{nf}}{(C_p)_{nf}\mu_{nf}}\theta''=0\end{cases}\tag{4}$$

The effective dynamic viscosity μ_{nf} and thermal conductivity k_{nf} of nanofluid have been defined on the basis of the Brinkman's law and Maxwell's model, respectively. Brinkman's law for the viscosity of nanofluid is $\mu_{nf}=\dfrac{\mu_f}{(1-\phi)^{2.5}}$, where ϕ is the nanoparticles volume fraction. Maxwell's model for thermal conductivity of nanofluid is $k_{nf}=k_f\left[1+\dfrac{3\phi(k_p/k_f-1)}{k_p/k_f+2-\phi(k_p/k_f-1)}\right]$, where k_p and k_f are the thermal conductivities of nanoparticles and base fluid.

At the same time kinematic viscosity of nanofluid can be defined as

$$\upsilon_{nf} = \frac{\mu_{nf}}{\rho_{nf}} = \frac{\mu_f}{(1-\phi)^{2.5}\left[\rho_p\phi + \rho_f(1-\phi)\right]}.$$

Some other parameters of nanofluid are given by following formulas:

$$(C_p)_{nf} = (C_p)_f(1-\phi) + (C_p)_p\phi$$

$$(\rho\beta)_{nf} = (\rho\beta)_f(1-\phi) + (\rho\beta)_p\phi$$

$$\rho_{nf}\beta_f = \beta_f\left(\rho_f(1-\phi) + \rho_p\phi\right)$$

$$\frac{(\rho\beta)_{nf}}{\rho_{nf}\beta_f} = \frac{(\rho\beta)_f(1-\phi) + (\rho\beta)_p\phi}{\beta_f\left(\rho_f(1-\phi) + \rho_p\phi\right)} = \frac{1-\phi+\phi\dfrac{(\rho\beta)_p}{(\rho\beta)_f}}{1-\phi+\phi\dfrac{\rho_p}{\rho_f}}$$

Here also we have the following boundary conditions:

$$\begin{aligned} &\eta = 0: \ f = 0,\ f' = 0,\ \theta = 1, \\ &\eta \to \infty: \ f' = 0,\ \theta = 0. \end{aligned} \tag{5}$$

The formulated boundary-value problem (4) and (5) has been solved using an in-house computational code (Runge–Kutta method of the fourth order with shooting technique [25, 26]) and also using the Matlab software (function BVP4C) [26].

2.1.2. Double-phase model

In this part of thesis, we used the mathematical nanofluid model proposed by Buongiorno [20] to study the problem of natural convection of nanofluid from an isothermal vertical flat plate. On the basis of scale analysis, the standard boundary-layer approximation was taken into account and then we obtained the following governing equations:

$$\frac{\partial u}{\partial x} + \frac{\partial v}{\partial y} = 0 \tag{6}$$

$$\mu\frac{\partial^2 u}{\partial y^2} - \rho_f\left(u\frac{\partial u}{\partial x} + v\frac{\partial u}{\partial y}\right) + \left[(1-\phi_\infty)\rho_{f\infty}\beta g(T-T_\infty) - (\rho_p - \rho_{f\infty})g(\phi-\phi_\infty)\right] = 0 \tag{7}$$

$$u\frac{\partial T}{\partial x}+v\frac{\partial T}{\partial y}=\alpha\frac{\partial^2 T}{\partial y^2}+\tau\left[D_B\frac{\partial \phi}{\partial y}\frac{\partial T}{\partial y}+\left(\frac{D_T}{T_\infty}\right)\left(\frac{\partial T}{\partial y}\right)^2\right] \quad (8)$$

$$u\frac{\partial \phi}{\partial x}+v\frac{\partial \phi}{\partial y}=D_B\frac{\partial^2 \phi}{\partial y^2}+\left(\frac{D_T}{T_\infty}\right)\frac{\partial^2 T}{\partial y^2} \quad (9)$$

The next step of our research is to transform the partial differential governing equations into non-dimensional ordinary differential governing equations using four similarity variables given by:

$$\eta=\frac{y}{x}\left(\frac{Gr_x}{4}\right)^{1/4},\ \psi=4vf(\eta)\left(\frac{Gr_x}{4}\right)^{1/4},\ \theta=\frac{T-T_\infty}{T_w-T_\infty},\ S=\frac{\phi-\phi_\infty}{\phi_w-\phi_\infty}$$

The derivatives of velocities and temperature are then derived from the above similarity variables as following:

$$u=\frac{\partial \psi}{\partial y}=\frac{4v}{x}\left(\frac{Gr_x}{4}\right)^{1/2}f'$$

$$v=-\frac{\partial \psi}{\partial x}=-\frac{v}{x}\left(\frac{Gr_x}{4}\right)^{1/4}(-f'\eta+3f)$$

$$\frac{\partial u}{\partial x}=\frac{\partial^2 \psi}{\partial x\partial y}=\frac{v}{x^2}\left(\frac{Gr_x}{4}\right)^{1/2}(2f'-f''\eta),$$

$$\frac{\partial u}{\partial y}=\frac{\partial^2 \psi}{\partial y^2}=\frac{4v}{x^2}\left(\frac{Gr_x}{4}\right)^{3/4}f'',$$

$$\frac{\partial^2 u}{\partial y^2}=\frac{\partial^3 \psi}{\partial y^3}=\frac{vGr_x}{x^3}f''',$$

$$\frac{\partial T}{\partial x}=\frac{\partial \theta}{\partial x}(T_w-T_\infty)=\frac{\theta'}{-4x}\eta(T_W-T_\infty)$$

$$\frac{\partial T}{\partial y}=\frac{\partial \theta}{\partial y}(T_w-T_\infty)=\frac{\theta'}{x}\left(\frac{Gr_x}{4}\right)^{1/4}(T_W-T_\infty)$$

$$\frac{\partial^2 T}{\partial y^2}=\frac{\partial^2 \theta}{\partial y^2}(T_w-T_\infty)=\theta''\frac{1}{x^2}\left(\frac{Gr_x}{4}\right)^{1/2}(T_W-T_\infty)$$

$$\frac{\partial \phi}{\partial y}=S'\frac{1}{x}\left(\frac{Gr_x}{4}\right)^{1/4}(\phi_w-\phi_\infty)$$

$$\frac{\partial \phi}{\partial x}=\frac{-S'}{4x}\eta(\phi_w-\phi_\infty)$$

$$\frac{\partial^2 \phi}{\partial y^2} = S'' \frac{1}{x^2}\left(\frac{Gr_x}{4}\right)^{1/2}\left(\phi_w - \phi_\infty\right)$$

Substituting all of the above terms to governing equations (6)–(9) we will obtain the following equations:

– PDE (7) becomes an ODE:

$$\frac{\rho_{f\infty}}{\rho_f} f''' + 3ff'' - 2\left(f'\right)^2 + \frac{(1-\phi_\infty)\rho_{f\infty}}{\rho_f}\theta - \frac{(1-\phi_\infty)\rho_{f\infty}}{\rho_f} Nr \cdot S = 0$$

Taking into account that $\rho_{f\infty} = \rho_f$ and $\phi_\infty = 0$, then we obtain:

$$f''' + 3ff'' - 2\left(f'\right)^2 + \theta - Nr \cdot S = 0,$$

where $Nr = \dfrac{(\rho_p - \rho_{f\infty})(\phi_w - \phi_\infty)}{\rho_{f\infty}\beta(T_w - T_\infty)(1-\phi_\infty)}$

– PDE (8) becomes:

$$\theta'' + 3\mathrm{Pr} \cdot f \cdot \theta' + N_b S'\theta' + N_t\left(\theta'\right)^2 = 0,$$

where $N_b = \dfrac{\left(\rho c\right)_p D_B\left(\phi_w - \phi_\infty\right)}{\left(\rho c\right)_f \alpha}$, $N_t = \dfrac{\left(\rho c\right)_p D_T\left(T_w - T_\infty\right)}{\left(\rho c\right)_f \alpha T_\infty}$, $Pr = \dfrac{\nu}{\alpha}$.

– PDE (9) becomes:

$$S'' + 3Pr \cdot Le \cdot f \cdot S' + \frac{N_t}{N_b}\theta'' = 0,$$

where $Le = \dfrac{\alpha}{D_B}$.

Then we obtain the system of ODEs:

$$\begin{cases} f''' + 3ff'' - 2\left(f'\right)^2 + \theta - Nr \cdot S = 0 \\ \theta'' + 3Pr \cdot f \cdot \theta' + N_b S'\theta' + N_t\left(\theta'\right)^2 = 0 \\ S'' + 3Pr \cdot Le \cdot f \cdot S' + \dfrac{N_t}{N_b}\theta'' = 0 \end{cases} \tag{10}$$

Boundary conditions can be written as follows:

$$\begin{aligned} &\eta = 0: \ f = 0,\ f' = 0,\ \theta = 1,\ S = 1 \\ &\eta \to \infty: \ f' = 0,\ \theta = 0,\ S = 0. \end{aligned} \tag{11}$$

It should be noted that this formulated boundary-value problem (10) and (11) has been solved using the Matlab software (function BVP4C) [26].

2.2. Full Navier-Stokes equations (single-phase model)

Within this part we have a system of partial differential equations for nanofluid near the vertical isothermal plate taking into account the single-phase model [22–24]:

$$\frac{\partial u}{\partial x}+\frac{\partial v}{\partial y}=0 \tag{12}$$

$$\rho_{nf}\left(\frac{\partial u}{\partial t}+u\frac{\partial u}{\partial x}+v\frac{\partial u}{\partial y}\right)=-\frac{\partial p}{\partial x}+\mu_{nf}\nabla^2 u \tag{13}$$

$$\rho_{nf}\left(\frac{\partial v}{\partial t}+u\frac{\partial v}{\partial x}+v\frac{\partial v}{\partial y}\right)=-\frac{\partial p}{\partial y}+\mu_{nf}\nabla^2 v+\left(\rho\beta\right)_{nf} g\left(T-T_\infty\right)$$

(14)

$$\left(\rho C_p\right)_{nf}\left(\frac{\partial T}{\partial t}+u\frac{\partial T}{\partial x}+v\frac{\partial T}{\partial y}\right)=k_{nf}\nabla^2 T \tag{15}$$

The next step is to reduce the system of four equations to a system of three equations by introducing two new variables (ψ, ω). These new functions ψ and ω are given by the following formula:

$$u=\frac{\partial \psi}{\partial y},\ v=-\frac{\partial \psi}{\partial x},\ \omega=\frac{\partial v}{\partial x}-\frac{\partial u}{\partial y} \tag{16}$$

Consequently, u and v in Eqs. (12)–(15) are replaced by ψ and ω. We obtain a system of three equations as following [24]:

$$\nabla^2\psi=-\omega \tag{17}$$

$$\frac{\partial \omega}{\partial t}+u\frac{\partial \omega}{\partial x}+v\frac{\partial \omega}{\partial y}=\frac{\mu_{nf}}{\rho_{nf}}\nabla^2\omega+\frac{\left(\rho\beta\right)_{nf}}{\rho_{nf}}g\frac{\partial T}{\partial x} \tag{18}$$

$$\left(\rho C_p\right)_{nf}\left(\frac{\partial T}{\partial t}+u\frac{\partial T}{\partial x}+v\frac{\partial T}{\partial y}\right)=k_{nf}\nabla^2 T \tag{19}$$

Then the system of three equations is reduced to non-dimensional form by using the following relations:

$$X=\frac{x}{L},\ Y=\frac{y}{L},\ \tau=\frac{t}{t_0},\ U=\frac{u}{V_0},\ V=\frac{v}{V_0},\ \Theta=\frac{T-T_0}{\Delta T},\ \Psi=\frac{\psi}{\psi_0},\ \Omega=\frac{\omega}{\omega_0}$$

where $\Delta T=T_w-T_0,\ V_0=\sqrt{g\beta\Delta TL},\ \psi_0=V_0L,\ \omega_0=\frac{V_0}{L}$.

Therefore, non-dimensional equations for our problem are given by [24]:

$$\nabla^2\Psi=-\Omega \tag{20}$$

$$\frac{\partial\Omega}{\partial\tau}+U\frac{\partial\Omega}{\partial X}+V\frac{\partial\Omega}{\partial Y}=\frac{\mu_{nf}}{\rho_{nf}}\frac{\rho_f}{\mu_f}\sqrt{\frac{Pr}{Ra}}\nabla^2\Omega+\frac{(\rho\beta)_{nf}/(\rho\beta)_f}{\rho_{nf}/\rho_f}\frac{\partial\Theta}{\partial X} \tag{21}$$

$$\frac{\partial\Theta}{\partial\tau}+U\frac{\partial\Theta}{\partial X}+V\frac{\partial\Theta}{\partial Y}=\frac{k_{nf}/k_f}{(\rho C_p)_{nf}/(\rho C_p)_f}\frac{1}{\sqrt{Ra\cdot\mathrm{Pr}}}\nabla^2\Theta \tag{22}$$

In order to exclude the effect of boundary conditions these equations have been solved in the following domain of interest (see Fig. 3):

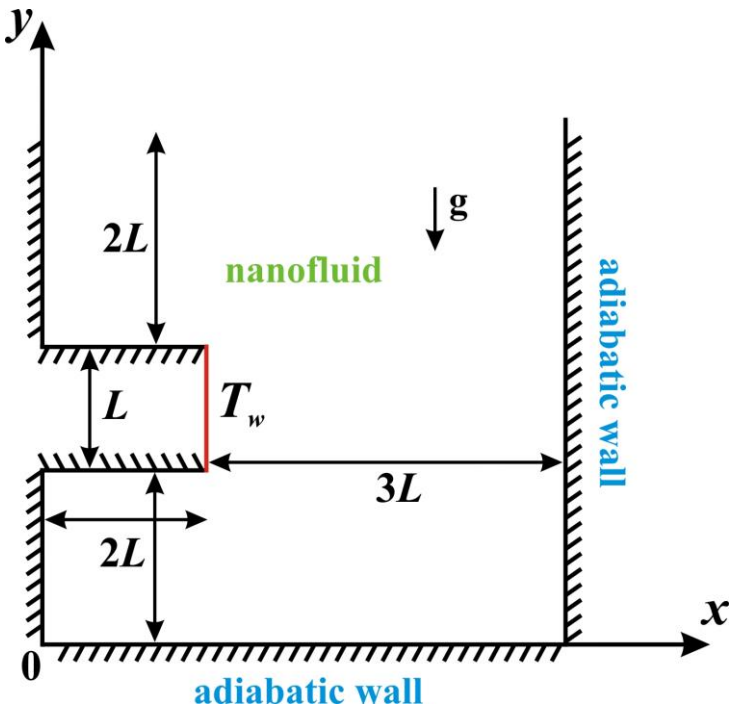

Fig. 3. *Physical model for full Navier–Stokes equations*

with the following boundary conditions

$$\Psi=0,\frac{\partial\Psi}{\partial\mathbf{n}}=0 \text{ at all rigid walls,}$$

$\frac{\partial \Theta}{\partial \mathbf{n}} = 0$ at all walls except for the isothermal plate, where $\Theta = 1$,

$\frac{\partial \Psi}{\partial y} = \frac{\partial \Omega}{\partial y} = \frac{\partial \Theta}{\partial y} = 0$ at outlet (Y = 5).

In order to solve the formulated boundary-value problem for governing equations (20)–(22) we use the finite difference method of the second order accuracy. To approximate differential equations by FDM, we introduce a space-time grid with coordinates: $x_i = i \cdot h$, $y_j = j \cdot l$, $\tau_n = n \cdot \Delta\tau$, where h, l are the grid steps along x, y coordinates, respectively; $\Delta\tau$ is the time step; $i = \overline{0, M}$; $j = \overline{0, N}$; $n = \overline{0, K}$

We introduce the following notation: $\Omega(ih, jl, n\Delta\tau) = \Omega_{i,j}^n$.

Taking into account the approximations of derivatives with respect to spatial and time variables, the equations (20)–(22) then become using the locally one-dimensional Samarskiy scheme [24]:

$$\frac{\Psi_{i+1,j}^n - 2\Psi_{i,j}^n + \Psi_{i-1,j}^n}{h^2} + \frac{\Psi_{i,j+1}^n - 2\Psi_{i,j}^n + \Psi_{i,j-1}^n}{l^2} = -\Omega_{i,j}^n \tag{23}$$

$$\frac{\Omega_{i,j}^{n+\frac{1}{2}} - \Omega_{i,j}^n}{\Delta\tau} + U_{i,j}\frac{\Omega_{i+1,j}^{n+\frac{1}{2}} - \Omega_{i-1,j}^{n+\frac{1}{2}}}{2h} - U_{i,j}\frac{\Omega_{i+1,j}^{n+\frac{1}{2}} - 2\Omega_{i,j}^{n+\frac{1}{2}} + \Omega_{i-1,j}^{n+\frac{1}{2}}}{2h} =$$

$$= \frac{\mu_{nf}}{\rho_{nf}}\frac{\rho_f}{\mu_f}\sqrt{\frac{Pr}{Ra}}\left(1 + U_{i,j}\frac{h\frac{\mu_f}{\rho_f}\frac{\rho_{nf}}{\mu_{nf}}\sqrt{\frac{Ra}{Pr}}}{2}\right)^{-1}\frac{\Omega_{i+1,j}^{n+\frac{1}{2}} - 2\Omega_{i,j}^{n+\frac{1}{2}} + \Omega_{i-1,j}^{n+\frac{1}{2}}}{h^2} + \tag{24a}$$

$$+ \frac{(\rho\beta)_{nf}/(\rho\beta)_f}{\rho_{nf}/\rho_f}\frac{\Theta_{i+1,j}^n - \Theta_{i-1,j}^n}{2h}$$

$$\frac{\Omega_{i,j}^{n+1}-\Omega_{i,j}^{n+\frac{1}{2}}}{\Delta\tau}+V_{i,j}\frac{\Omega_{i,j+1}^{n+1}-\Omega_{i,j-1}^{n+1}}{2l}-V_{i,j}\frac{\Omega_{i,j+1}^{n+1}-2\Omega_{i,j}^{n+1}+\Omega_{i,j-1}^{n+1}}{2l}=$$

$$=\frac{\mu_{nf}}{\rho_{nf}}\frac{\rho_f}{\mu_f}\sqrt{\frac{Pr}{Ra}}\left(1+V_{i,j}\frac{l\frac{\mu_f}{\rho_f}\frac{\rho_{nf}}{\mu_{nf}}\sqrt{\frac{Ra}{Pr}}}{2}\right)^{-1}\frac{\Omega_{i,j+1}^{n+1}-2\Omega_{i,j}^{n+1}+\Omega_{i,j-1}^{n+1}}{l^2} \qquad (24b)$$

$$\frac{\Theta_{i,j}^{n+\frac{1}{2}}-\Theta_{i,j}^{n}}{\Delta\tau}+U_{i,j}\frac{\Theta_{i+1,j}^{n+\frac{1}{2}}-\Theta_{i-1,j}^{n+\frac{1}{2}}}{2h}-U_{i,j}\frac{\Theta_{i+1,j}^{n+\frac{1}{2}}-2\Theta_{i,j}^{n+\frac{1}{2}}+\Theta_{i-1,j}^{n+\frac{1}{2}}}{2h}=$$

$$=\frac{k_{nf}/k_f}{\left(\rho C_p\right)_{nf}/\left(\rho C_p\right)_f}\frac{1}{\sqrt{Ra\cdot Pr}}\left(1+U_{i,j}\frac{h\left(\rho C_p\right)_{nf}/\left(\rho C_p\right)_f\sqrt{Ra\cdot Pr}}{2k_{nf}/k_f}\right)^{-1}\times \qquad (25a)$$

$$\times\frac{\Theta_{i+1,j}^{n+\frac{1}{2}}-2\Theta_{i,j}^{n+\frac{1}{2}}+\Theta_{i-1,j}^{n+\frac{1}{2}}}{h^2}$$

$$\frac{\Theta_{i,j}^{n+1}-\Theta_{i,j}^{n+\frac{1}{2}}}{\Delta\tau}+V_{i,j}\frac{\Theta_{i,j+1}^{n+1}-\Theta_{i,j-1}^{n+1}}{2l}-V_{i,j}\frac{\Theta_{i,j+1}^{n+1}-2\Theta_{i,j}^{n+1}+\Theta_{i,j-1}^{n+1}}{2l}=$$

$$=\frac{k_{nf}/k_f}{\left(\rho C_p\right)_{nf}/\left(\rho C_p\right)_f}\frac{1}{\sqrt{Ra\cdot Pr}}\left(1+V_{i,j}\frac{l\left(\rho C_p\right)_{nf}/\left(\rho C_p\right)_f\sqrt{Ra\cdot Pr}}{2k_{nf}/k_f}\right)^{-1}\times \qquad (25b)$$

$$\times\frac{\Theta_{i,j+1}^{n+1}-2\Theta_{i,j}^{n+1}+\Theta_{i,j-1}^{n+1}}{l^2}$$

The difference Poisson's equation (23) has been solved by successive over relaxation method [24]. The difference equations for Ω and Θ have been solved by Thomas algorithm [24].

3. VALIDATION AND VERIFICATION

3.1. Free convection of clear fluid near vertical isothermal wall

For the first benchmark problem we analyzed natural convection of clear fluid from an isothermal vertical flat plate. To verify our results, we make a comparison between Jaluria's results [22] and data of Crepeau and Clarksean [27]. We calculated the dimensionless velocity profiles of clear fluid at different values of Prandtl number ranging from 0.01 to 1000. Velocity increases sharply at the areas near to the wall and reach maximum value within the boundary layer, then it gradually deceases to zero.

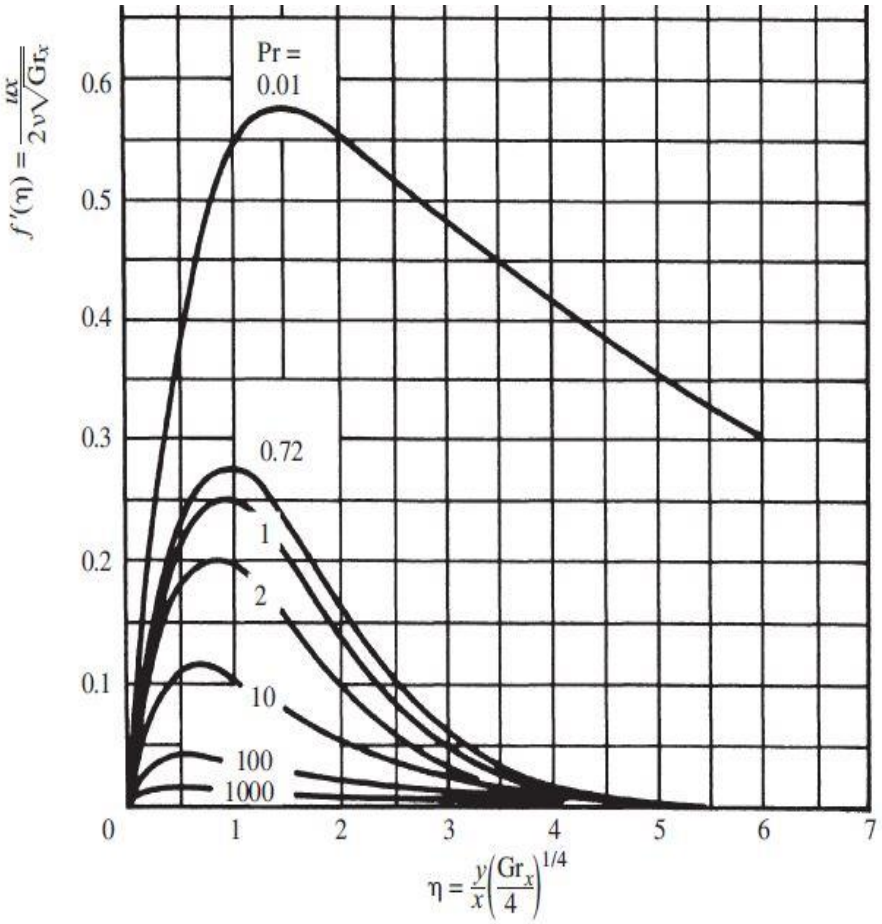

Fig. 4 . *Velocity profiles for clear fluids with different Prandtl numbers* [22]

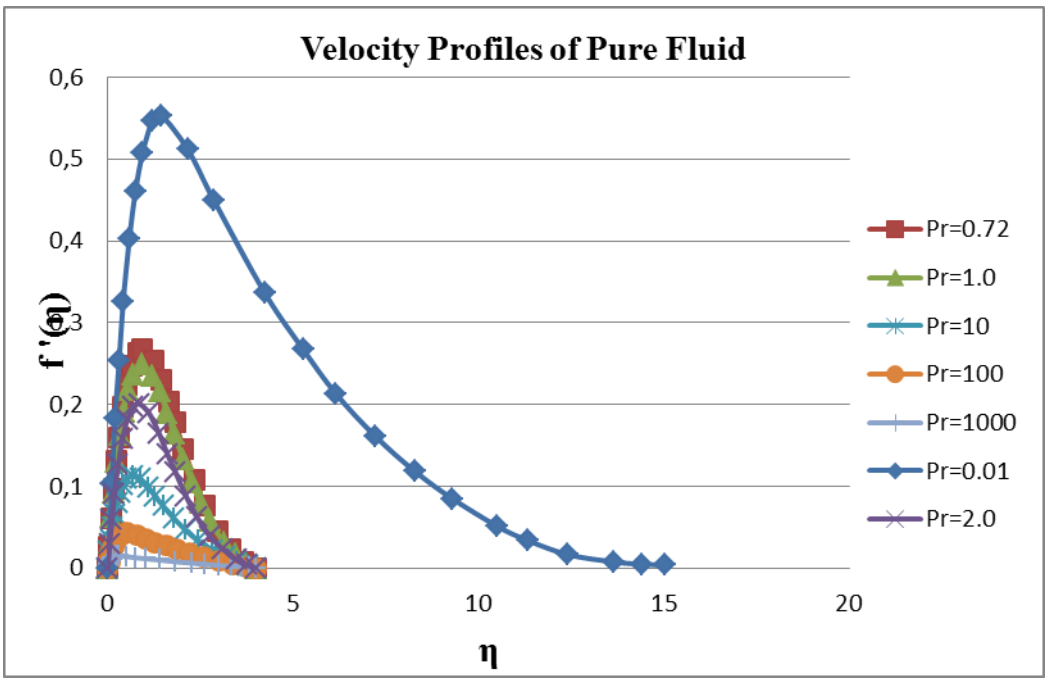

Fig. 5. *Obtained velocity profiles for clear fluids with various Prandtl numbers*

An increase of velocity near the wall can be explained by convective heat transfer of fluid from the hot wall. In Figs. 4 and 5 we can see a very good agreement between the present results and results calculated by Jaluria [22].

Table 2 shows good comparison for temperature gradients with data of Crepeau and Clarksean [27].

Table 2. Comparison with results by Crepeau and Clarksean [27]

Pr	θ′ at η = 0 [27]	θ′ at η = 0 (present results)
0.001	-0.0264	-0.0278
0.01	-0.08059	-0.0809
0.1	-0.2302	-0.2305
1	-0.5671	-0.5671
10	-1.169	-1.169
100	-2.191	-2.1895

3.2. Free convection of nanofluid near vertical isothermal wall

The next benchmark problem was natural convective heat transfer of nanofluid near the vertical isothermal wall using the double-phase model [28, 29]. Fig. 6 shows comparison of the velocity profiles at $Pr = 10$, $Le = 10$, $Nr = N_b = N_t = 0.5$ with data of Kuznetsov and Nield [28]. It is clear that the velocity profiles are the same in both cases. In addition, a velocity comparison between the present results and results conducted by Ibrahim and Makinde [29] has been carried out in Fig. 7 (at $Nr = 0.3$) and Fig. 8 (at $Nr = 0.6$). The difference between two researchs is that Ibrahim and Makinde [29] take into account the stratification constants ($\varepsilon_1 = \varepsilon_2 = 0.2$), meanwhile we do not consider stratification constants, namely, in our analysis $\varepsilon_1 = \varepsilon_2 = 0.0$. It can be seen in Figs. 7 and 8 that the velocity profiles of present result are significantly higher than the velocity profiles in the case of research by Ibrahim and Makinde [29]. Therefore, this leads to a conclusion that velocity magnitude decreases with stratification constants.

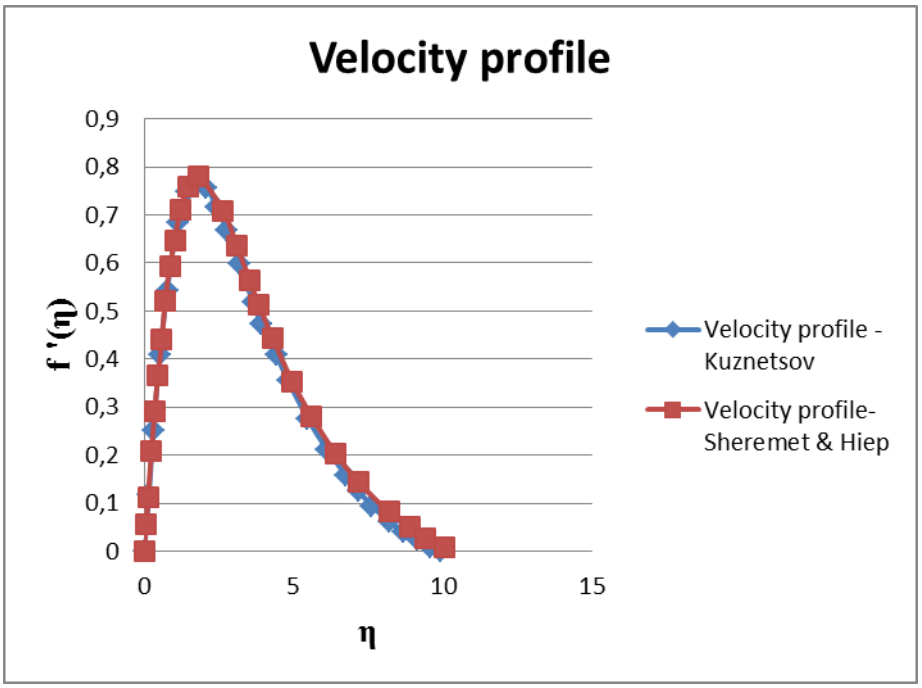

Fig. 6. *Comparison of velocity profiles between Kuznetsov and Nield* [28] *and present results for* $Pr = 10$, $Le = 10$, $Nr = N_b = N_t = 0.5$

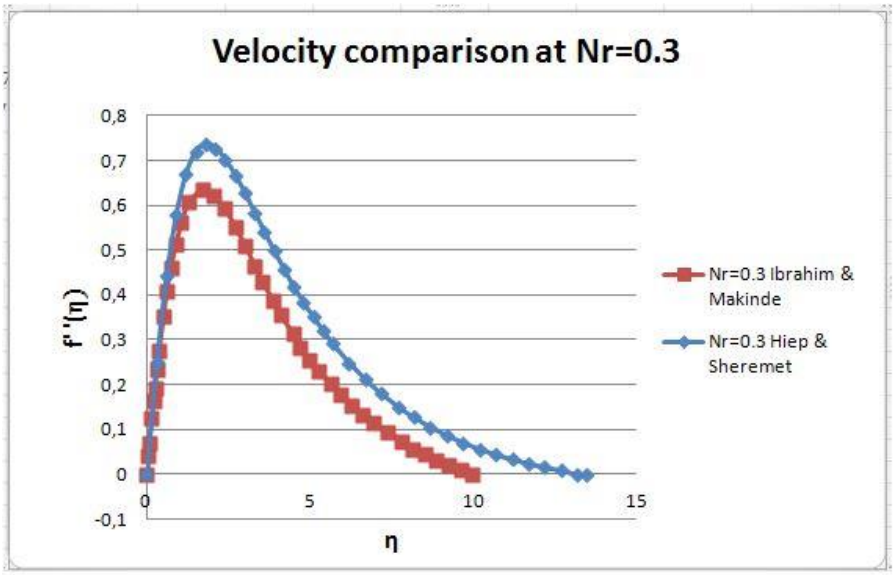

Fig. 7. *Comparison of velocity profiles between present result and Ibrahim and Makinde data [29] for* Pr = 10, Le = 2, Nr = 0.3, $N_b = N_t$ =0.5

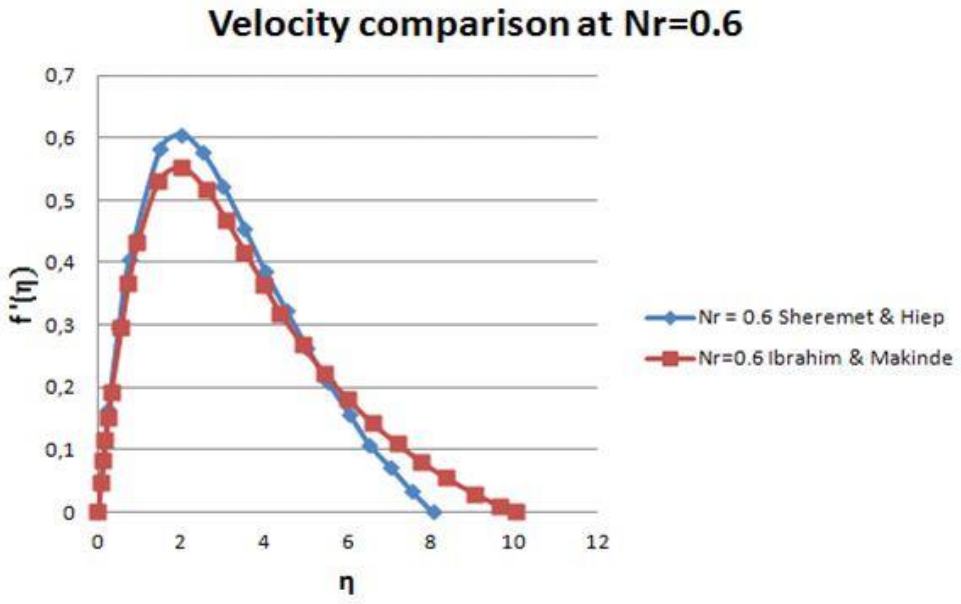

Fig. 8. *Comparison of velocity profiles between present result and Ibrahim and Makinde data [29] for* Pr = 10, Le = 2, Nr = 0.6, $N_b = N_t$ =0.5

3.3. Natural convection of nanofluid within differentially heated cavity

The third benchmark problem is a natural convection of nanofluid in a differentially heated cavity [30, 31].We compare our results with experimental [31] and numerical [30] studies of other authors. Table 3 gives the average Nusselt number for different nanoparticles volume concentration. It can be clearly seen that the results obtained using an in-house computational code agree well, which demonstrates the accuracy of the present code for nanofluid simulation.

Table 3. Comparison of average Nusselt number for natural convection of nanofluid in a differentially heated square cavity

			Average Nusselt number			
ϕ	*Ra*	*Pr*	Ho et al. [31]	Present study (FDM)	Saghir et al. [30] (FDM)	Saghir et al. [30] (FEM)
1 %	7.74547×10^{7}	7.0659	32.2037	30.6533	30.657	31.8633
2 %	6.6751180×10^{7}	7.3593	31.0905	30.5038	30.503	31.6085
3 %	5.6020687×10^{7}	7.8353	29.0769	30.2157	30.205	28.216

4. RESULTS AND DISCUSSION

4.1. Boundary-layer approach

4.1.1. Single-phase model

The results for temperature and velocity profiles are shown in Figs. 9 and 10 respectively. Temperature of nanofluid decreases from the vertical flat plate to the ambient environment and reaches zero value at a distance of approximately 1.5 from the vertical wall. This gradient of temperature is due to the difference between temperature of hot wall and temperature of ambient environment. Dimensionless velocity increases sharply near the wall and reaches the maximum value before going down gradually until become zero at η near to value of 4.

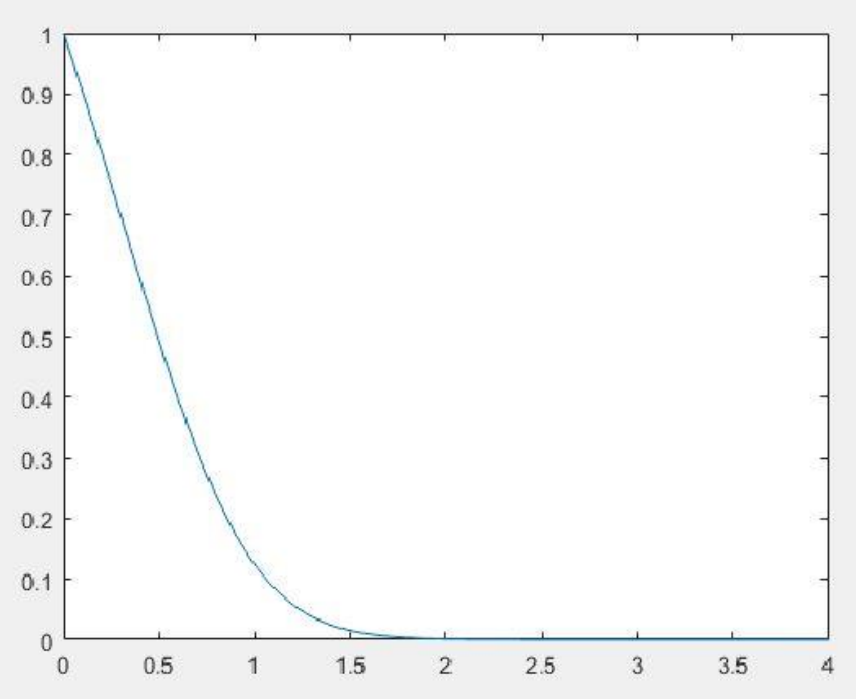

Fig. 9. *Temperature profile* θ(η) *for single-phase model*

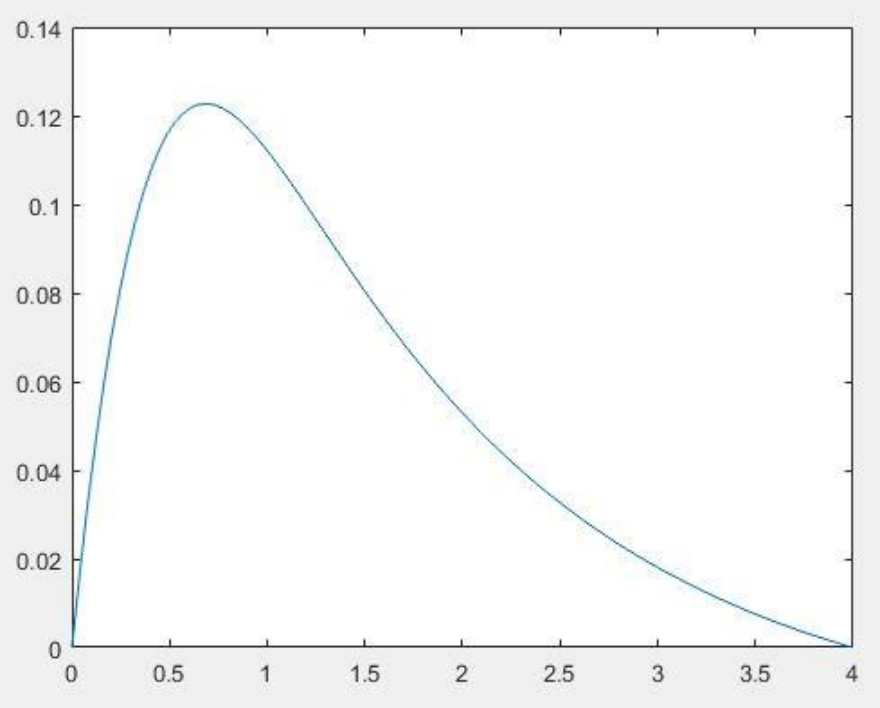

Fig. 10. *Velocity profile* $f'(\eta)$ *for single–phase model*

In Figs. 11 and 12 we showed the effect of different viscosity models on results of temperature and velocity profiles. In this simulation, we use following two viscosity models for nanofluids:

Brinkman's model: $\mu_{nf} = \dfrac{\mu_f}{(1-\phi)^{2.5}}$ [32] and model A: $\mu_{nf} = \mu_f\left(1+7.3\phi+123\phi^2\right)$ [33].

Although, the temperature profiles are equivalent for two models, a significant difference between velocity of Brinkman's model and velocity of model A has been observed.

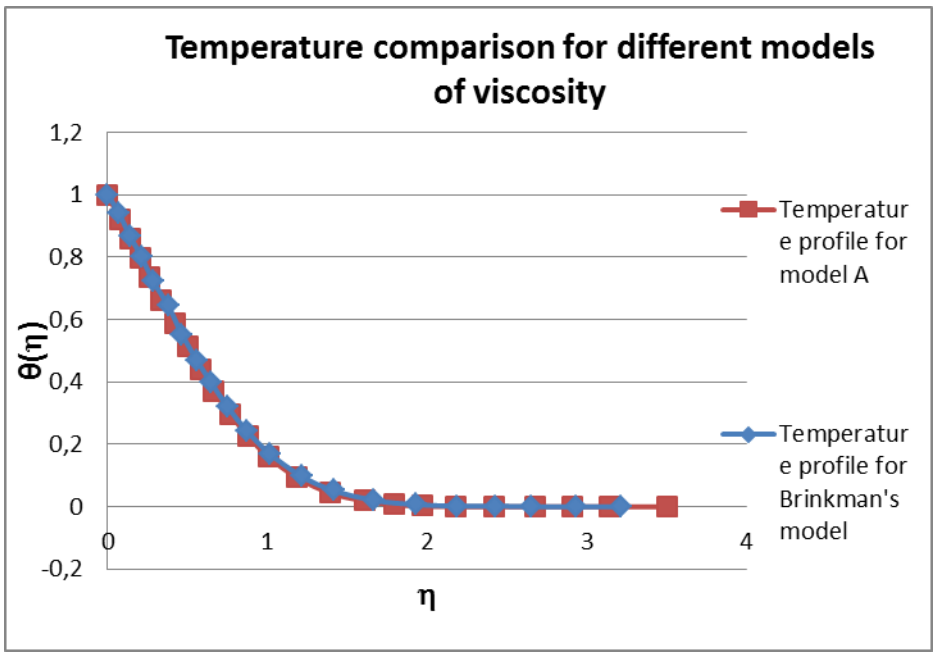

Fig. 11. *Comparison of temperature profiles for different models of nanofluid viscosity*

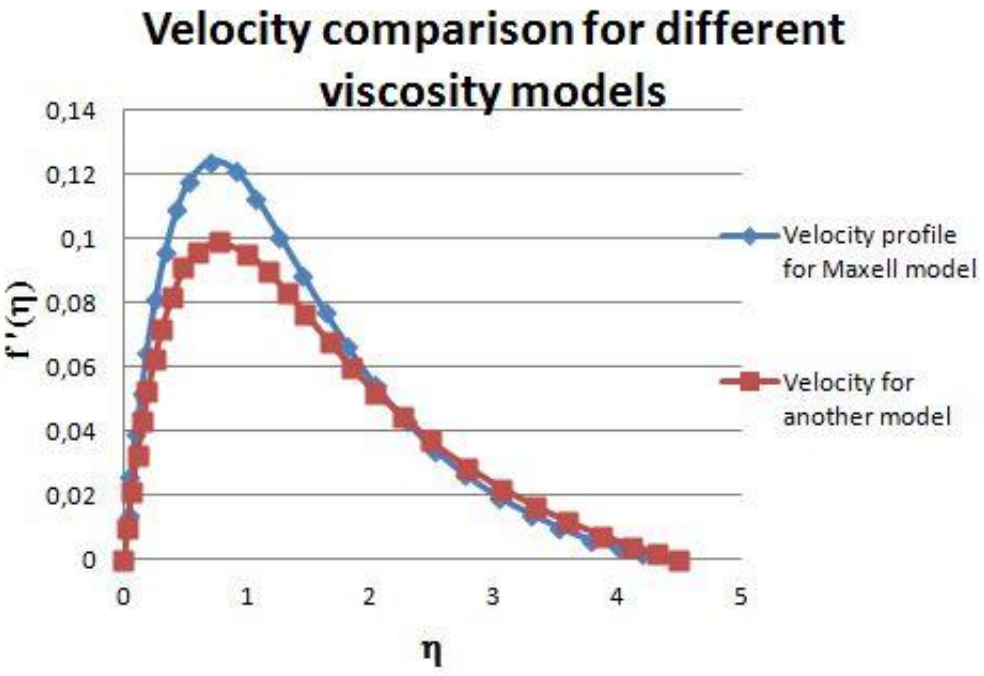

Fig. 12. *Comparison of velocity profiles for different models of nanofluid viscosity*

Different models for thermal conductivity coefficient are also taken into account. Effective thermal conductivities can be incorporated from the following

expressions corresponding to two types of nanoparticle shapes: spherical and cylindrical (nanotubes):

spherical nanoparticles – $\frac{k_{nf}}{k_f} = \frac{k_p + 2k_f - 2\phi\left(k_f - k_p\right)}{k_p + 2k_f + \phi\left(k_f - k_p\right)}$ and

cylindrical nanoparticles – $\frac{k_{nf}}{k_f} = \frac{k_p + 0.5k_f - 0.5\phi\left(k_f - k_p\right)}{k_p + 0.5k_f + \phi\left(k_f - k_p\right)}$.

Obviously, the profiles of velocity and temperature are unchanged regardless of different models for thermal conductivity as shown in Figs. 13 and 14. In the velocity profile, the maximum of velocity is obtained at $\eta \approx 1$ and the velocity boundary layer thickness is around $\eta \approx 4.5$. In Fig. 14 it is clear that temperature is a decreasing function of distance η from the wall to the tested position. The thermal boundary layer thickness is approximately $\eta \approx 2$.

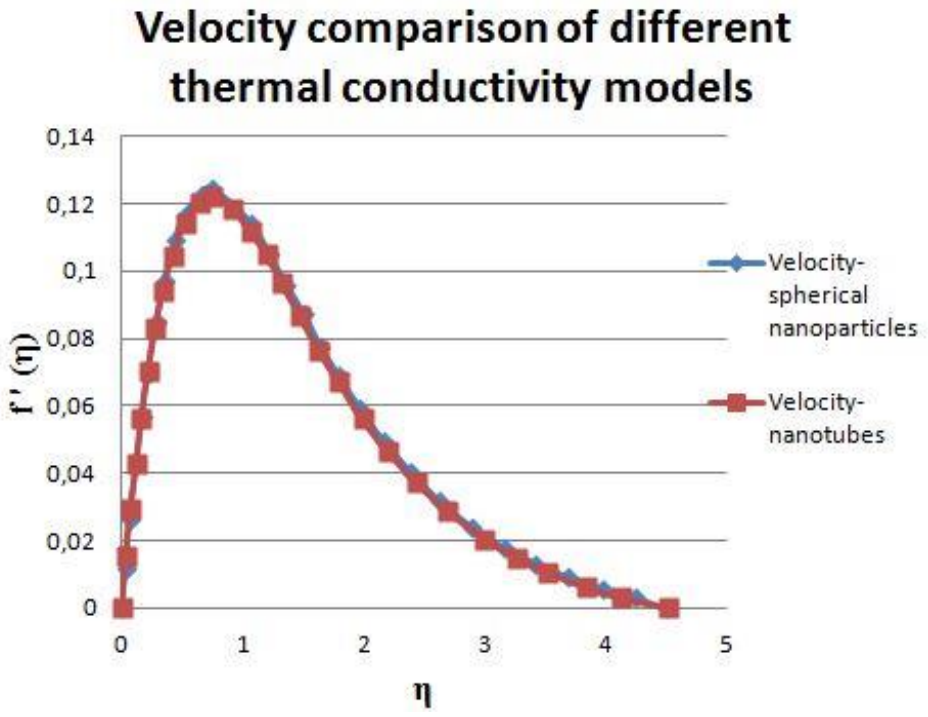

Fig. 13. *Velocity profiles for different models for thermal conductivity*

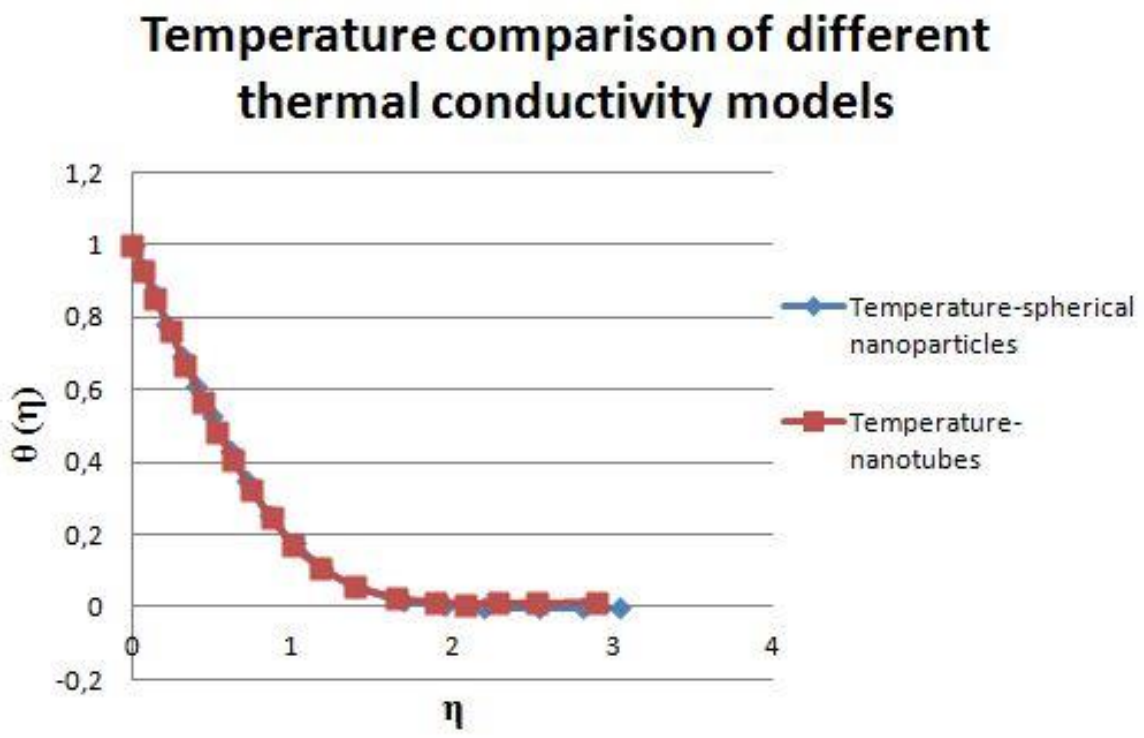

Fig. 14. *Temperature profiles for different models for thermal conductivity*

The effects of nanoparticles volume fraction in the range 0–4% and types of nanoparticles material (Ag, Cu, Al_2O_3, CuO, TiO_2) have been analyzed. A comparison between clear fluid and a nanofluid containing copper nanoparticles with concentration of 4% is also carried out. Profiles of dimensionless velocity and temperature at $\phi = 0.04$ are presented in Figs. 15 and 16 in comparison with clear fluid. An addition of nanoparticles inside the base fluid leads to the velocity reduction due to a growth of the dynamic viscosity. Meanwhile, it is clear in Fig. 16 that the thermal boundary layer of nanofluid increases in comparison with clear fluid.

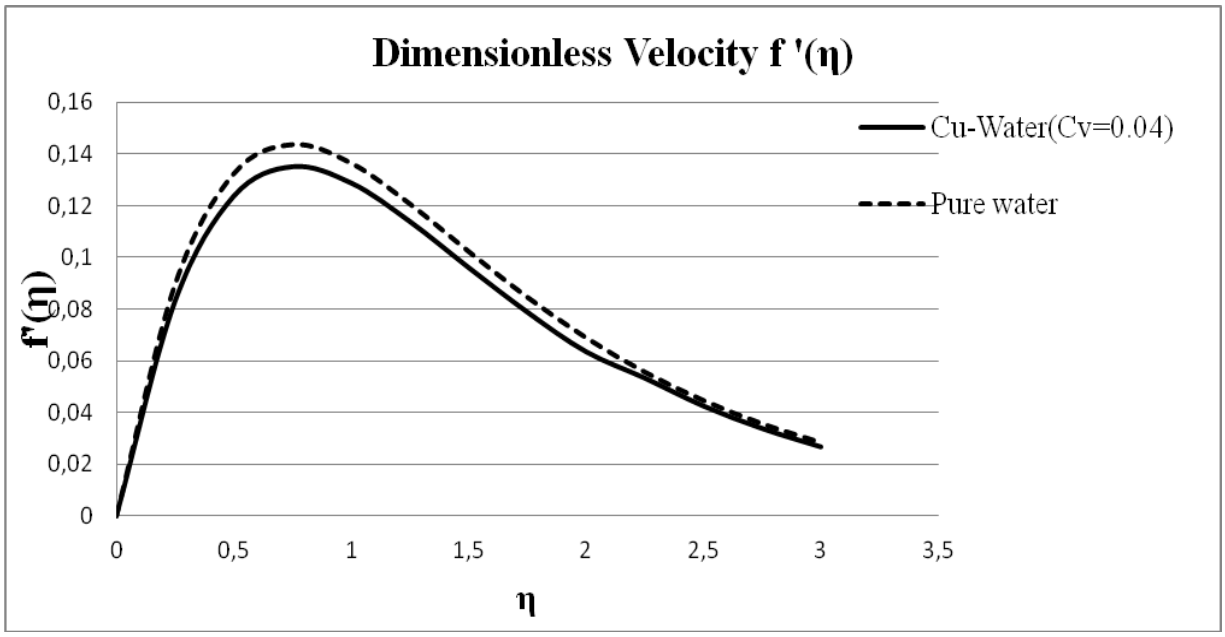

Fig. 15. *Velocity profiles for clear fluid and Cu-water nanofluid at $\phi = 0.04$*

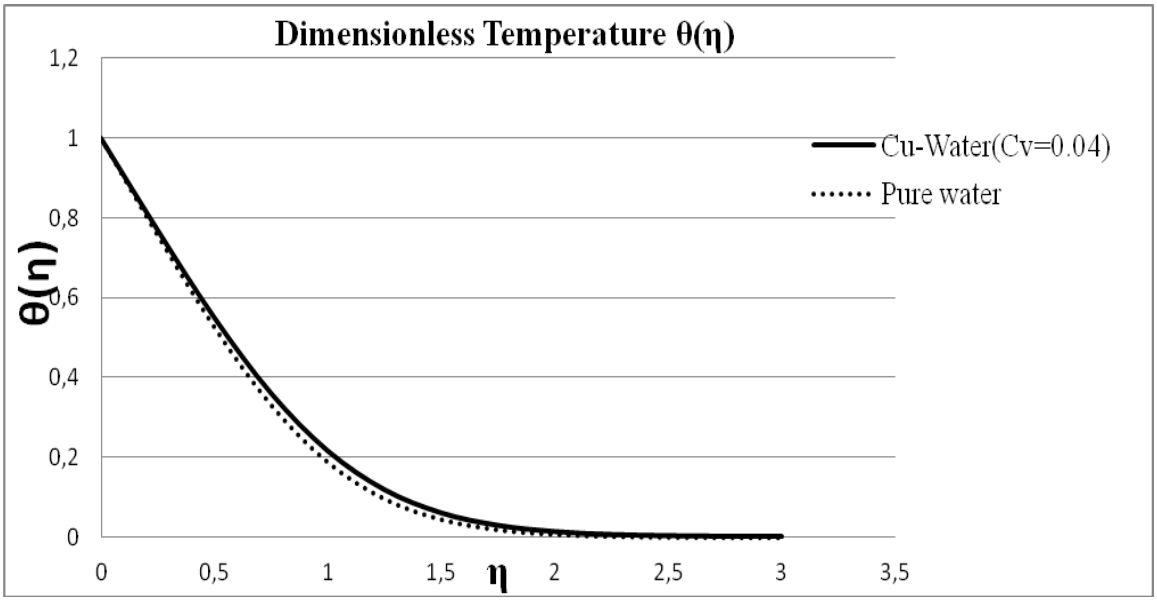

Fig. 16. *Temperature profiles for clear fluid and Cu-water nanofluid at $\phi = 0.04$*

Figure 17 compares velocity boundary layers of five types of nanofluids. Obviously, the velocity profiles vary with types of nanoparticles using for production of nanofluids. Firstly, the velocity decreases from Ag to TiO_2, then after some distance from the wall, the trend reverses.

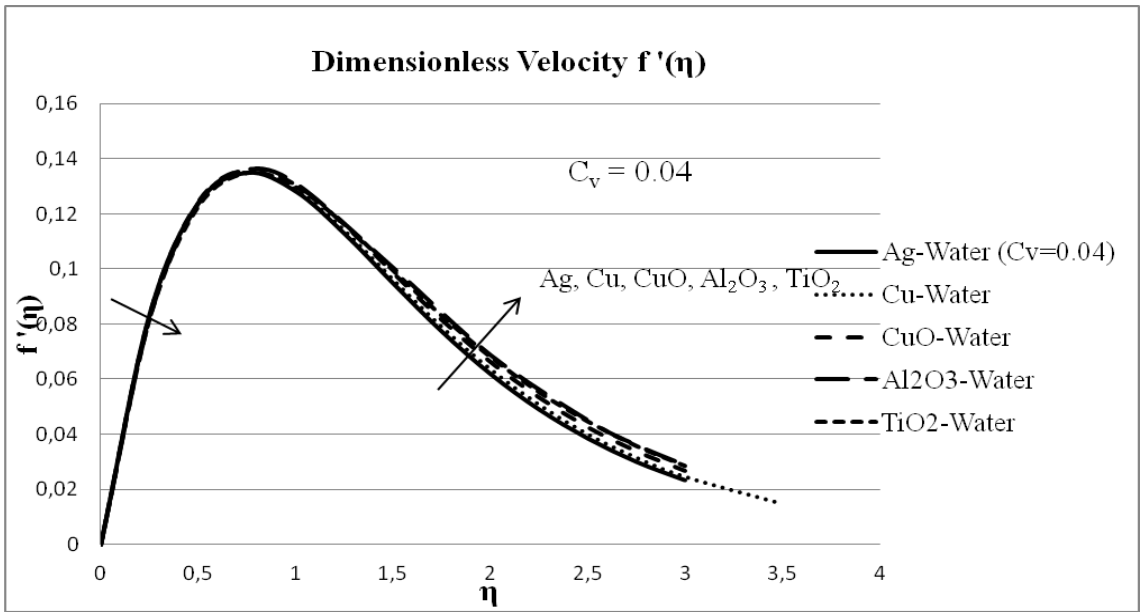

Fig. 17. *Variation in dimensionless velocity profiles of different nanofluids (Ag-water, Cu-water, CuO-water, Al_2O_3-water, TiO_2-water) with $\phi = 0.04$*

Table 4 describes results for reduced skin friction parameter of nanofluids for various ϕ in the range 0-4%. The reduced skin friction coefficient increases with higher value of concentration. Due to greater thermal conductivity, Cu-water and Ag-water nanofluids have the highest value of reduced skin friction number as compared to other nanofluids.

The reduced Nusselt numbers are performed in Table 5. With lower thermal conductivity of TiO_2, TiO_2-water nanofluid shows a smaller reduced Nusselt number. The higher concentrations of nanoparticles lead to a growth of the average Nusselt number. In the case of CuO-water nanofluid with $\phi = 0.04$, reduced Nusselt number increases by 7% as compared to clear water.

Table 4. Comparison of results for reduced skin friction number $C_f = \frac{1}{(1-\phi)^{2.5}} f''|_{\eta=0}$ for various ϕ

ϕ	Cu	CuO	Al_2O_3	TiO_2	Ag
0.0	0.4738	0.4738	0.4738	0.4738	0.4738
0.01	0.4757	0.4756	0.4748	0.4744	0.4762
0.02	0.4777	0.4775	0.4756	0.475	0.4788
0.03	0.4799	0.4795	0.4766	0.4756	0.4815
0.04	0.4821	0.4815	0.4774	0.4762	0.4844

Table 5. Comparison of results for reduced Nusselt number $Nu = -\frac{k_{nf}}{k_f}\theta'|_{\eta=0}$ for various ϕ

ϕ	Cu	CuO	Al_2O_3	TiO_2	Ag
0.0	0.9777	0.9777	0.9777	0.9777	0.9777
0.01	0.9937	0.9940	0.9939	0.9909	0.9934
0.02	1.0095	1.0001	1.0102	1.0043	1.0093
0.03	1.026	1.0272	1.0267	1.0177	1.0255
0.04	1.0425	1.0441	1.0430	1.0312	1.0418

4.1.2. Double-phase model

Numerical simulation in the case of double-phase model has been carried out at the following values of key parameters: Prandtl number (Pr = 7.0), Lewis number (2–1000), the buoyancy-ratio parameter (Nr = 0.2–2.0), the Brownian motion parameter (N_b = 0.2-2.0), the thermophoresis parameter (N_t = 0.1–2.0). In the case of double-phase model, we focus on the effects of these key parameters on the velocity profile, temperature profile and concentration profile of nanofluid. In Figs. 18–29, we can observe the effects of Nr, Le, N_b and N_t on velocity, temperature and concentration profiles. Figures 30–32 show us the results for

velocity, temperature and concentration profiles at different values of Brownian motion parameter and thermophoresis parameter such as $N_b = N_t = 0.001$, $N_b = N_t = 0.01$, $N_b = N_t = 0.1$ and $N_b = N_t = 0.5$.

It is obvious in Fig. 18 that velocity of nanofluid decreases with *Nr*. The peak of velocity moves far away from the wall when *Nr* increases. The velocity boundary layer thickness equals to $\eta \approx 4.5$ in all cases of *Nr*. Temperature increases with *Nr* (Fig. 19). It is also clear in Fig. 19 that the thermal boundary layer thickness increases with *Nr*. Concentration profile exhibits an increasing trend with *Nr* (Fig. 20). Therefore, the concentration boundary layer thickness increases as well. The increase of concentration boundary layer thickness can be explained by the motion of nanoparticles to quiescent fluid.

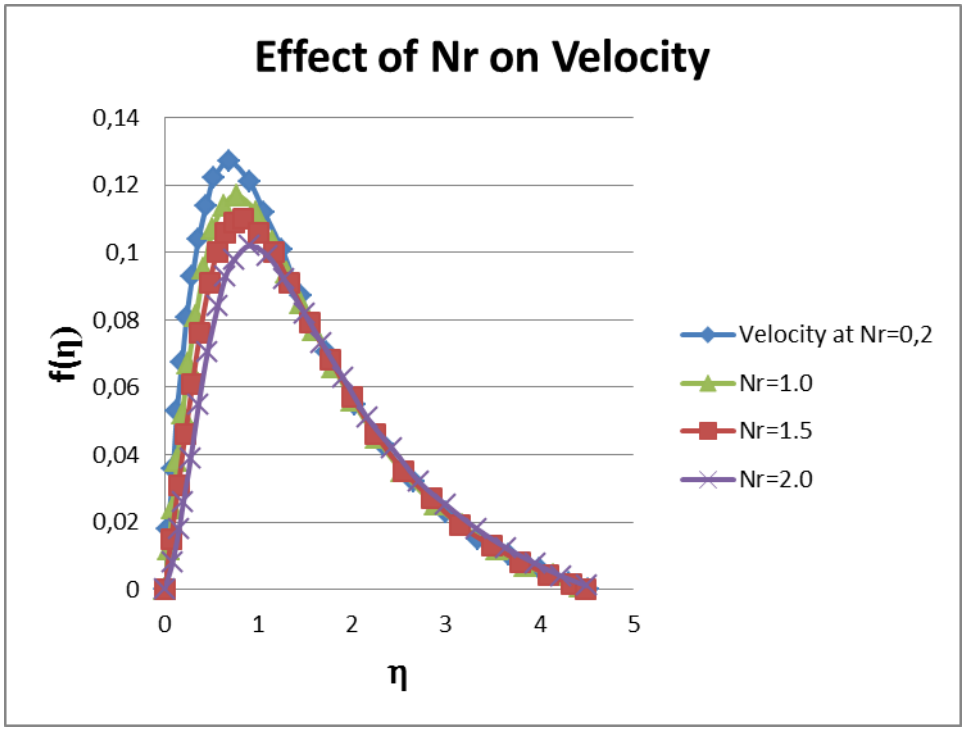

Fig. 18. *Effect of buoyancy-ratio parameter Nr on velocity profile*

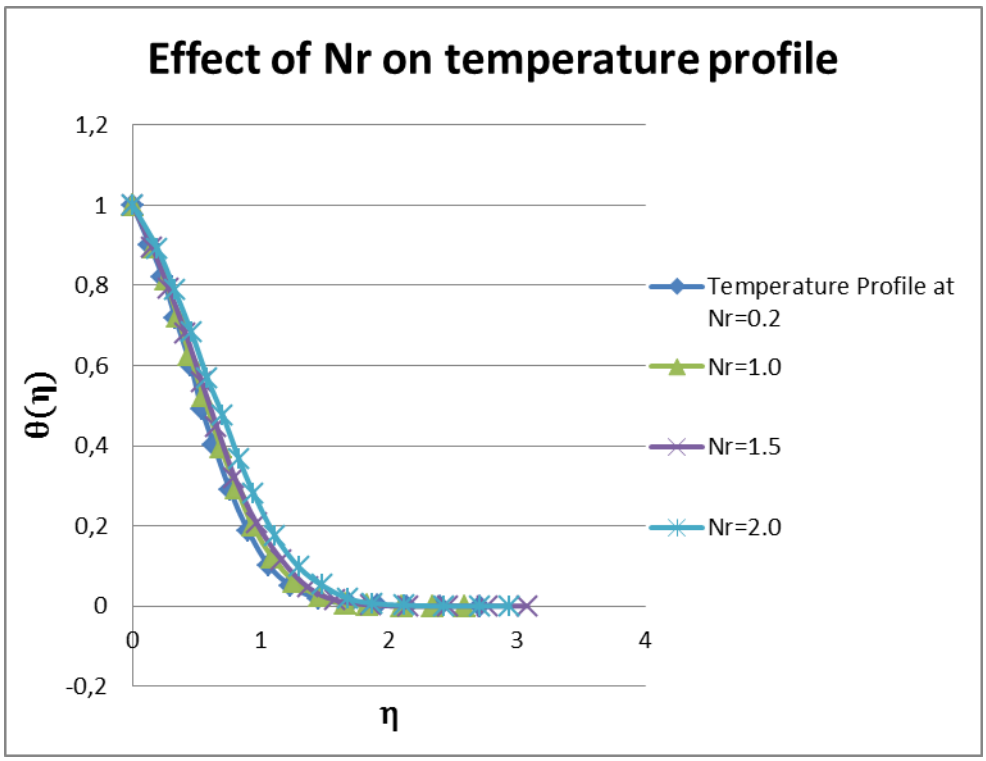

Fig. 19. *Effect of buoyancy-ratio parameter Nr on temperature profile*

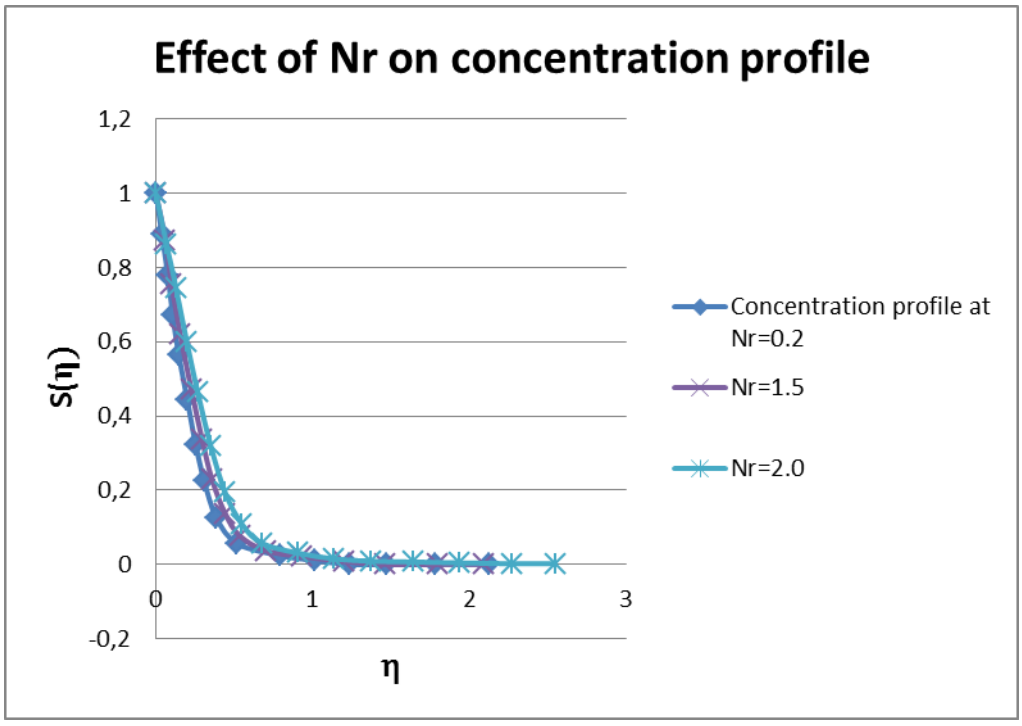

Fig. 20. *Effect of buoyancy-ratio parameter Nr on concentration profile*

We can see in Fig. 21 that the velocity profile increases when Lewis number increases. The peak of velocity moves close to the wall when Le increases. The temperature profile and concentration profile both decrease with Lewis number in

Figs. 22 and 23. Moreover, thermal boundary layer thickness and concentration boundary layer thickness are decreasing functions of *Le*.

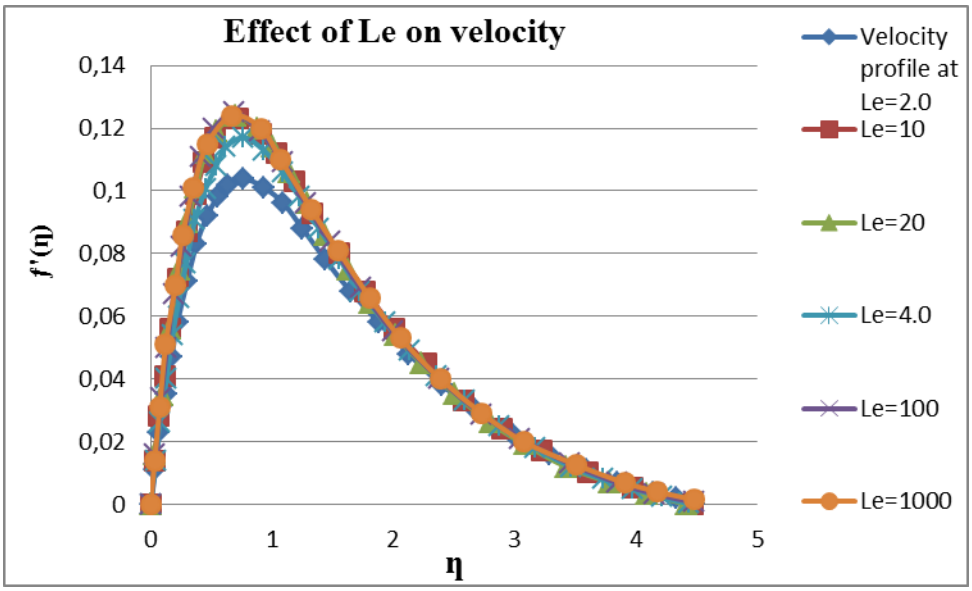

Fig. 21. *Effect of Lewis number Le on velocity profile*

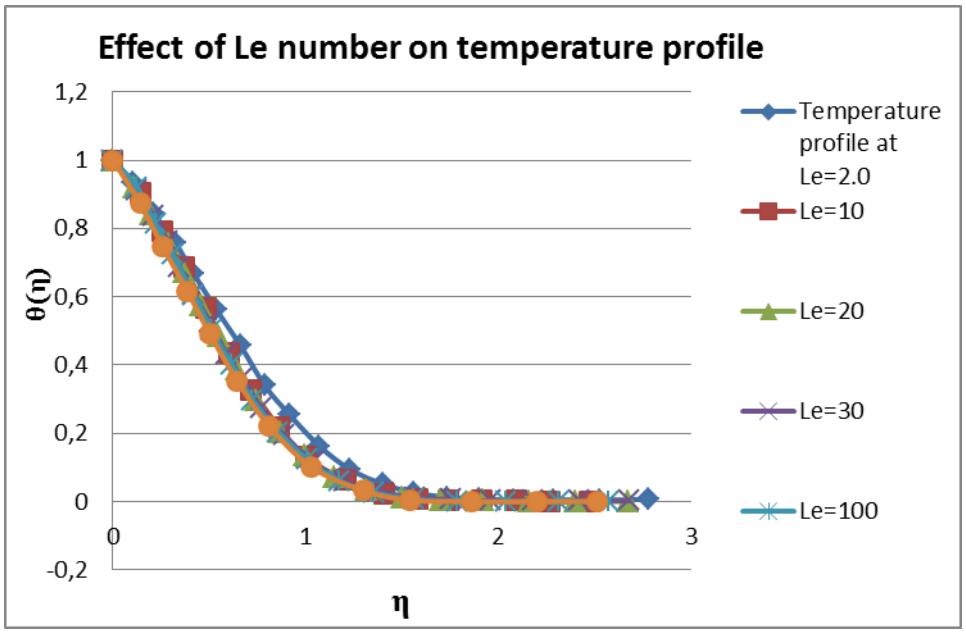

Fig. 22. *Effect of Lewis number Le on temperature profile*

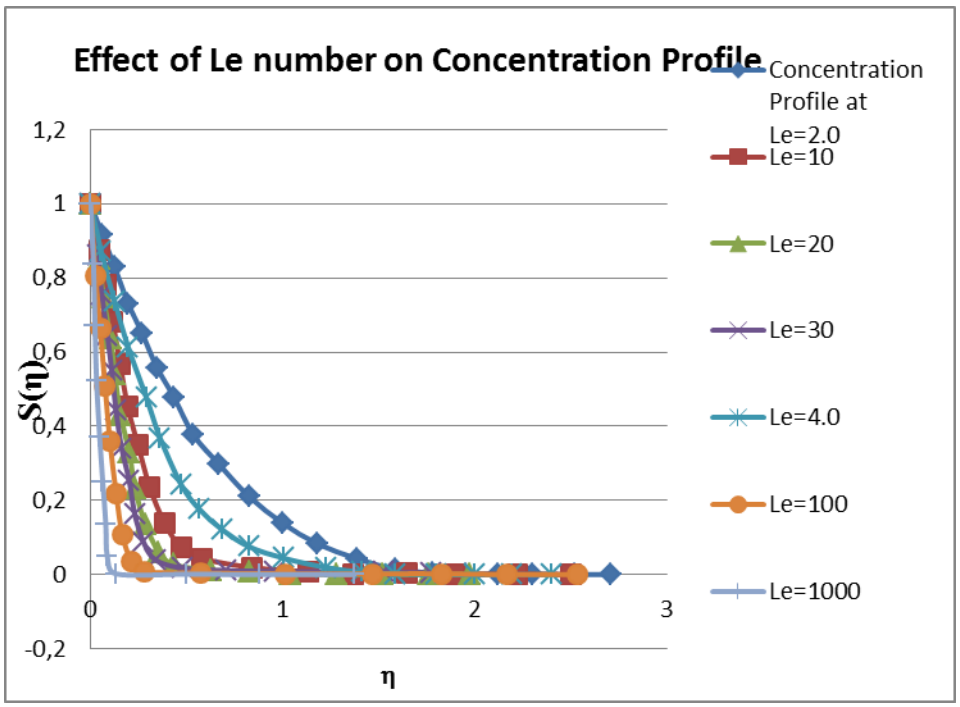

Fig. 23. *Effect of Lewis number Le on concentration profile*

Similarly, the temperature and velocity show a rising trend when N_t increases in Figs. 24 and 25. Therefore, the temperature of nanofluid increases with N_t. This increasing behavior of nanofluid temperature can be explained on the basis of thermophoresis mechanism. The thermophoresis mechanism takes into account the opposite motion of nanoparticles as compared to temperature gradient. The motion of nanoparticles to the ambient environment and greater temperature of nanoparticles make the greater temperature profile. It seems that the peak of velocity keep a constant distance from the wall regardless of different values of N_t. On the other hand, concentration profile increases with the change of thermophoresis number N_t (Fig. 26). This increase of concentration is a consequence of the motion of nanoparticles far away from greater temperature at the isothermal wall.

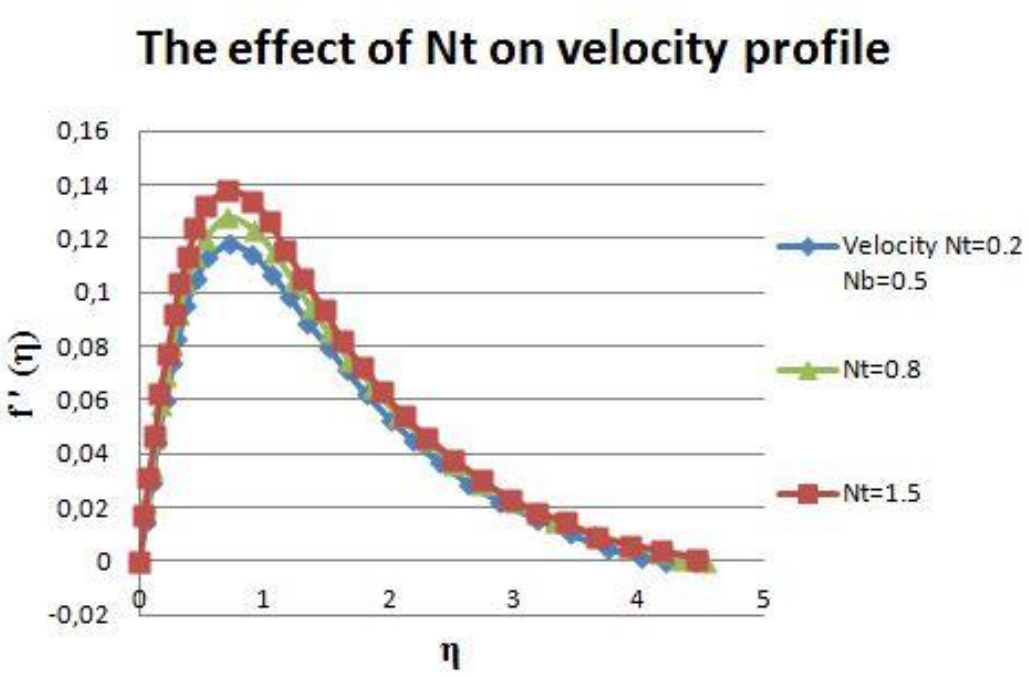

Fig. 24. *Effect of thermophoresis parameter N_t on velocity profile*

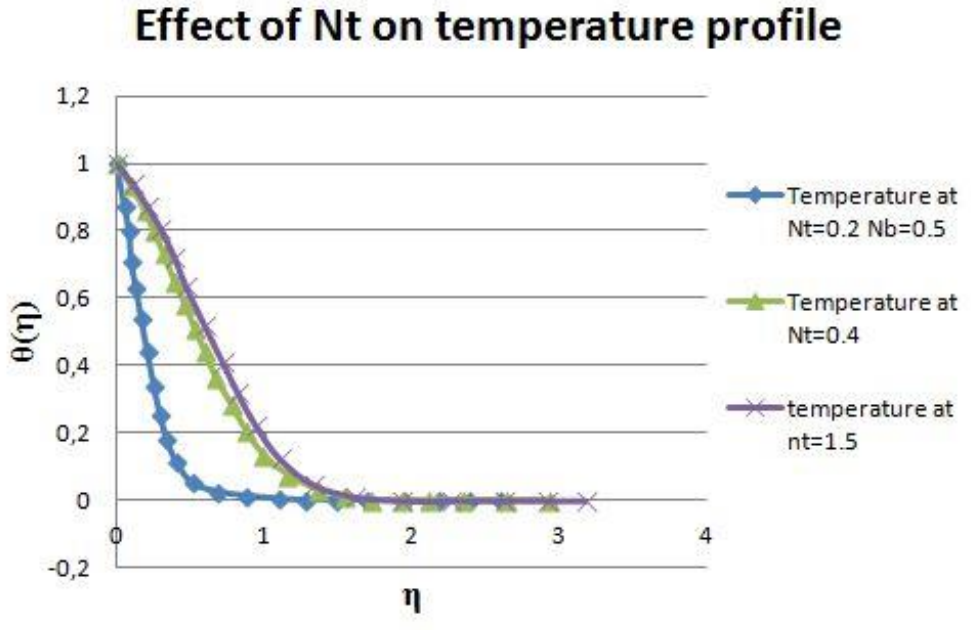

Fig. 25. *Effect of thermophoresis parameter N_t on temperature profile*

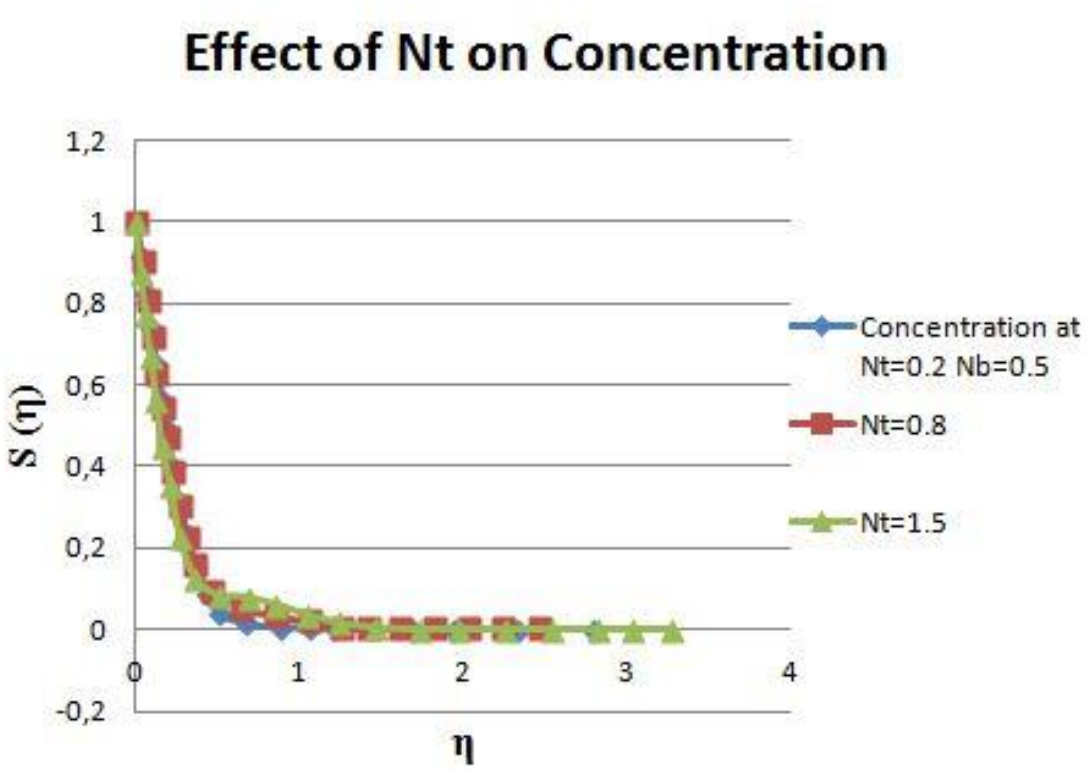

Fig. 26. *Effect of thermophoresis parameter N_t on concentration profile*

In Figs. 27–29 the effect of Brownian motion parameter N_b has been performed. It is clear that velocity increases, temperature remains unchanged and concentration shows a drop when N_b increases. The reduction of concentration with N_b can be explained by the motion of nanoparticles is opposite to motion of base fluid. Due to the decreasing trend of concentration profile with N_b, the concentration boundary layer thickness also decreases. The peak of velocity moves closely to the wall when N_b increases. The thermal boundary layer thickness is approximately at $\eta \approx 2$. The concentration boundary layer thickness decreases significantly with N_b. This can be as a consequence of the motion of nanoparticle opposite to motion of base fluid in effect of Brownian motion.

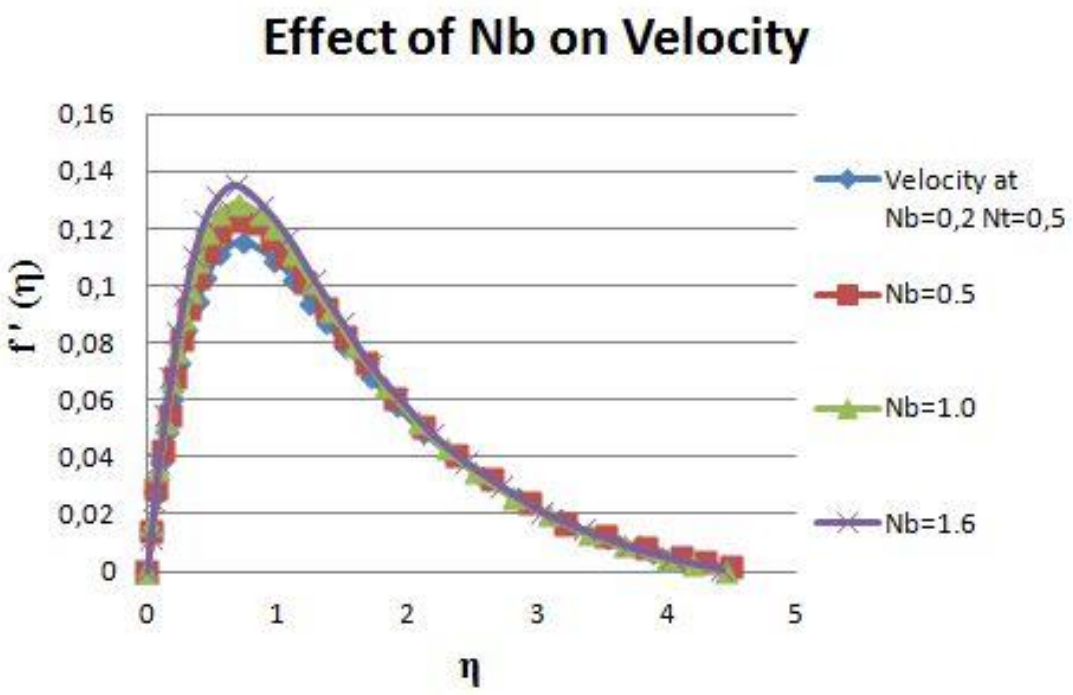

Fig. 27. *Effect of Brownian motion parameter N_b on velocity profile*

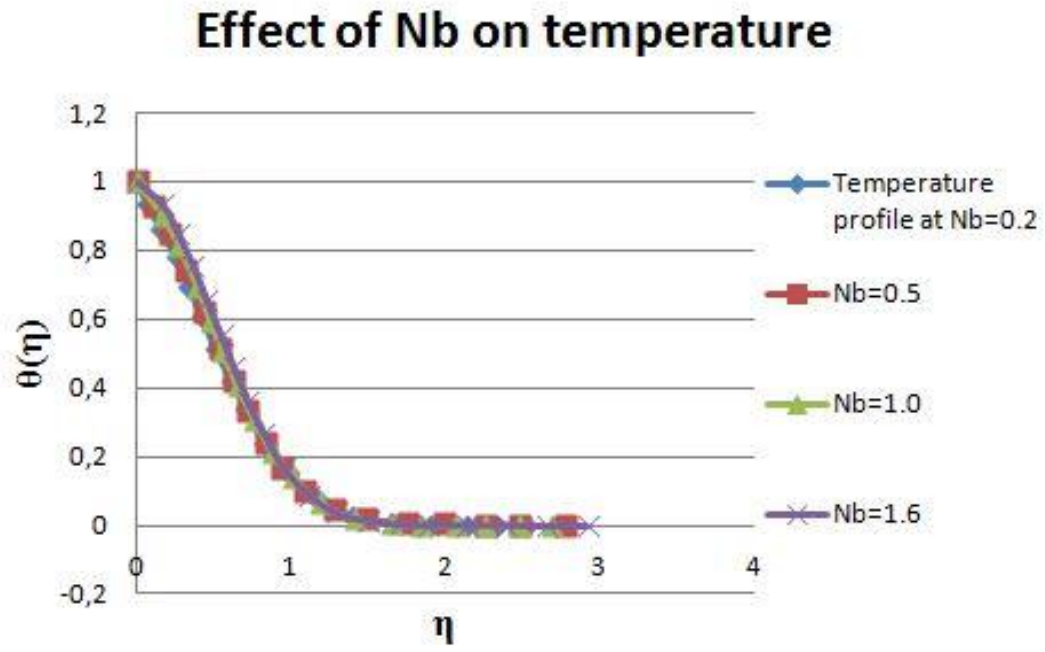

Fig. 28. *Effect of Brownian motion parameter N_b on temperature profile*

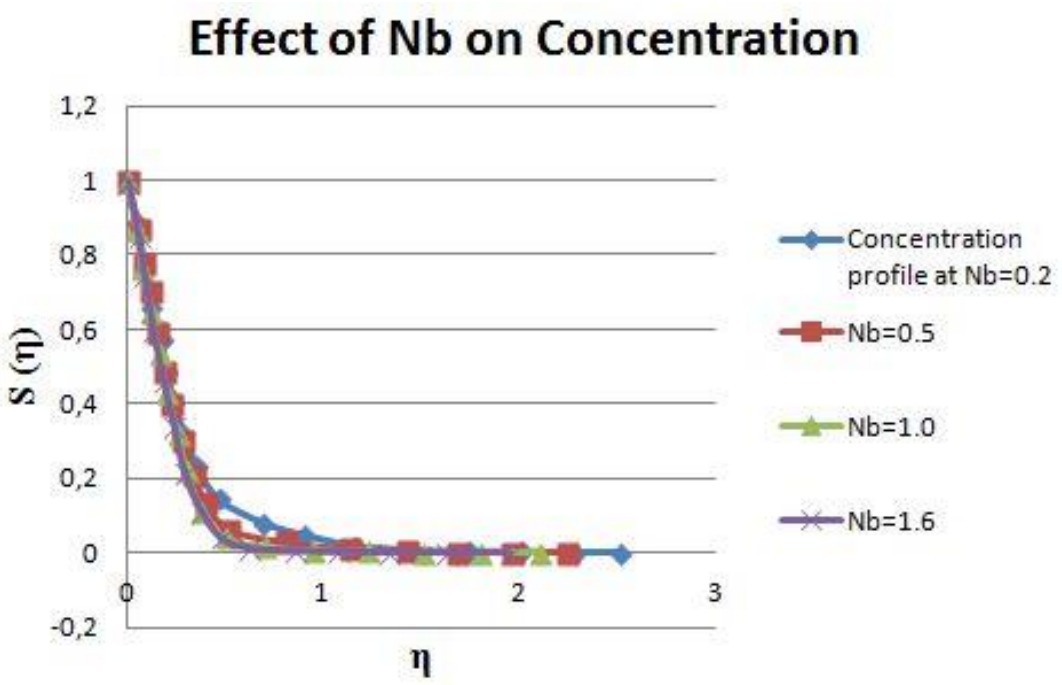

Fig. 29. *Effect of Brownian motion parameter N_b on concentration profile*

In Figs. 30–32 we study the effect of N_t and N_b in the range 0.001–0.5. The velocity profile increases with both N_t and N_b. The maximum of dimensionless velocity ranges from 0.1 to 0.12. The peak of velocity moves close to the hot wall when N_t and N_b increases. An increasing trend in temperature profile has been observed in Fig. 31. This trend is explained by the fact that temperature is an increasing function of both N_t and N_b as described in Figs. 25 and 28. The concentration profile nearly stays unchanged. This stable behavior of concentration is due to the fact that the increase of concentration with N_t cancels out the decrease of concentration with N_b. The thermal boundary layer thickness is approximately $\eta \approx 1.5$ and the concentration boundary layer thickness equals to $\eta \approx 1$.

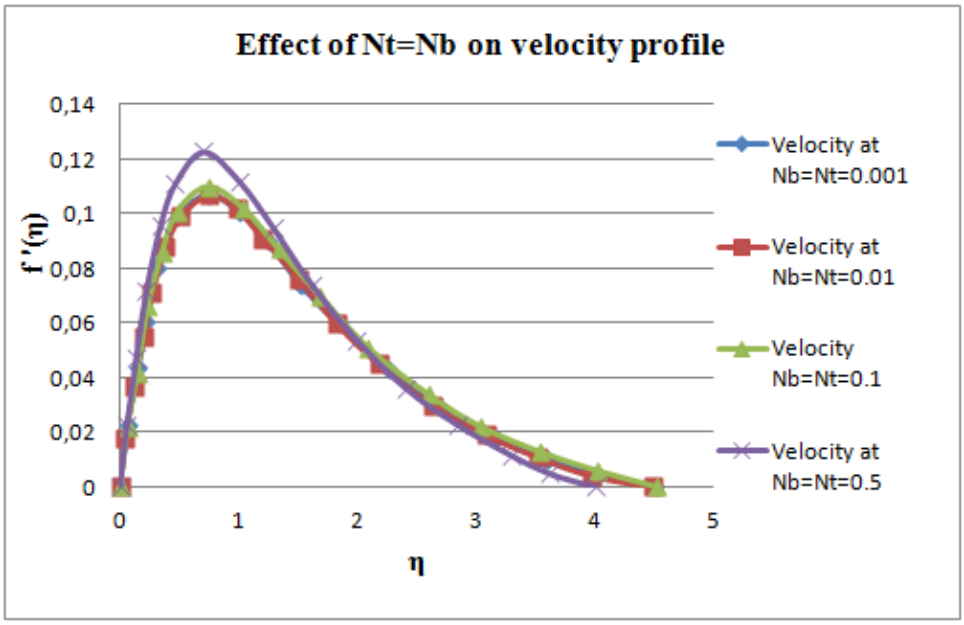

Fig. 30. *Effect of N_t and N_b in the range 0.001–0.5 on velocity profile*

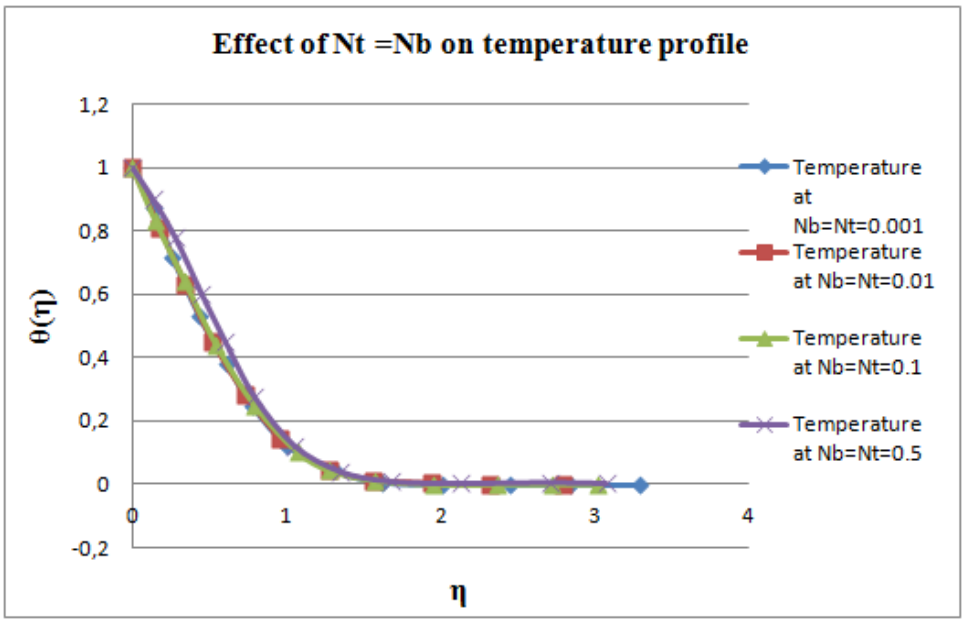

Fig. 31. *Effect of N_t and N_b in the range 0.001–0.5 on temperature profile*

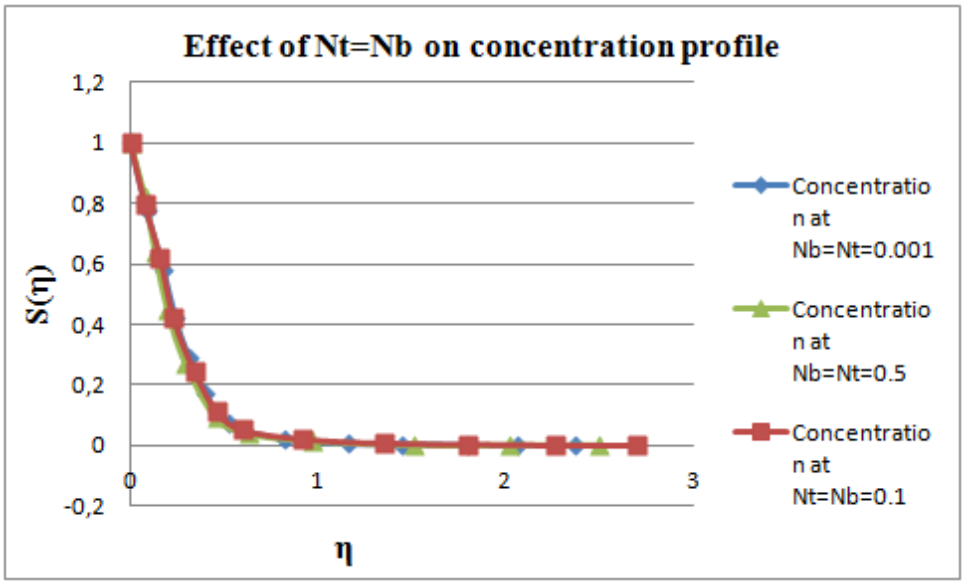

Fig. 32. *Effect of N_t and N_b in the range 0.001–0.5 on concentration profile*

4.2. Full Navier–Stokes equations (single-phase model)

Boundary-value problem (20)–(22) for the problem geometry (Fig. 3) have been solved for $Ra = 10^5$, $Pr = 0.7$, $\phi = 0.02$ and material nanoparticles is copper.

Figure 33 presents streamlines and isotherms near the isothermal vertical plate. One can find that due to convective heat transfer from the vertical wall, temperature of nanofluid near the wall is significantly higher than environmental temperature. It should be noted that near the heated wall the flow rises and the temperature is maximum.

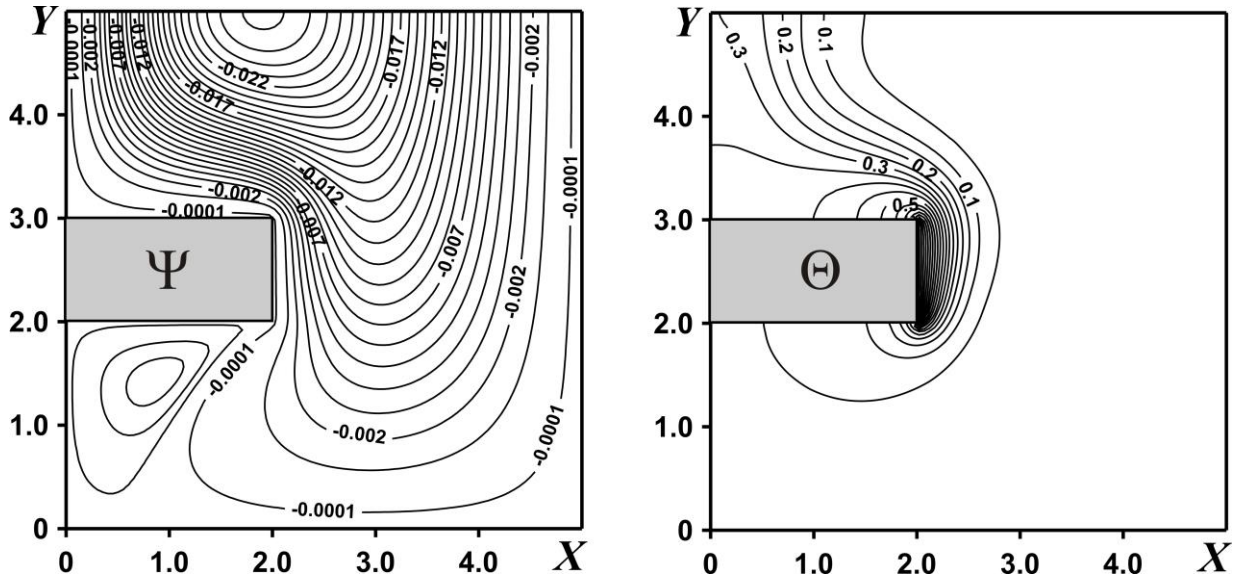

Fig. 33. *Streamlines and isotherms for $Ra=10^5$*

Also the gradients of stream function near the heated plate are greater than gradients of stream function at the areas far away from the wall. Therefore velocity increases to maximum and then decrease to minimum at the ambient environment. This behavior of velocity totally agrees with results in the cases of single-phase model and double-phase model for boundary-layer approach.

Profiles of velocity near the hot vertical plate are presented in Fig. 34 for different distance along the plate.

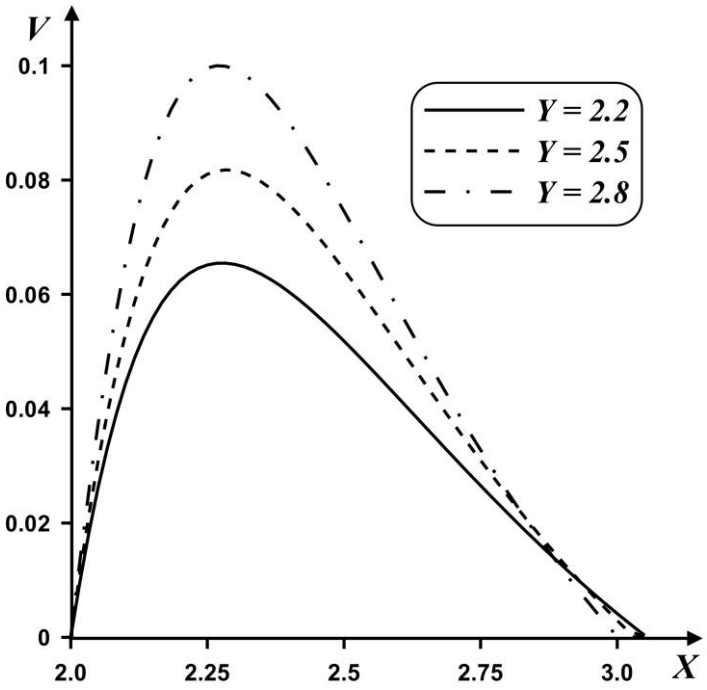

Fig. 34. *Velocity profiles for different values of Y*

4.3. Comparison between analyzed models

The problem of natural convection of nanofluid from an isothermal vertical flat plate using single-phase and double-phase models was studied within present thesis. Afterwards, the comparisons between two models have been carried out taking into account velocity profile and temperature profile.

Figures 35 and 36 present the agreement of results in the case of single-phase model and in the case of double-phase model taking into account $Pr = Le = 10$, $Nr = N_b = N_t = 0.5$. At the area near to isothermal wall, thermophoresis mechanism dominates Brownian motion; as a result, more amount of nanoparticles moves to a greater distance from the wall. Therefore temperature

of double-phase case is greater than temperature of single-phase one. At the area farther from isothemal wall, Brownian motion's role surpasses thermophoresis's role, this leads to lower temperature of double phase case.

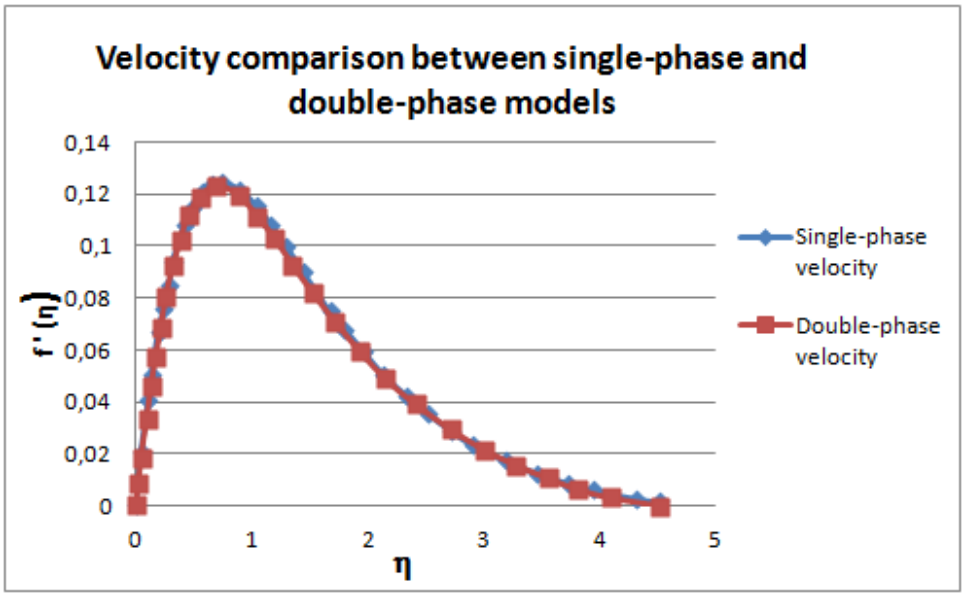

Fig. 35. *Velocity comparison at Pr = Le = 10, Nr = 0.5, $N_t = N_b$ =0.5*

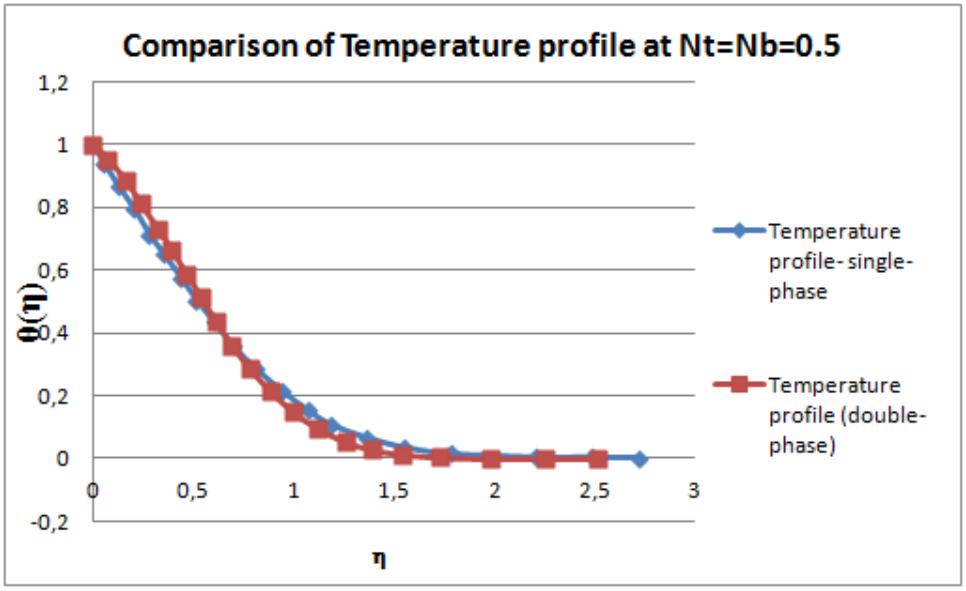

Fig. 36. *Temperature comparison at Pr = Le = 10, Nr = 0.5, $N_t = N_b$ =0.5*

7. CONCLUSIONS

Natural convection of nanofluid from an isothermal vertical flat plate has been studied numerically. Particular efforts have been focused on the effects of Lewis number, buoyancy-ratio parameter, Brownian motion parameter, thermophoresis parameter, different models of viscosity, different models of thermal conductivity and type of nanomaterials on velocity profile, temperature, nanoparticles volume fraction distributions, reduced Nusselt number and reduced skin friction number. It is found that the velocity profile of nanofluid is an increasing function of Lewis number, thermophoresis parameter and Brownian motion parameter, and a decreasing function of buoyancy-ratio parameter. The temperature profile is an increasing function of buoyancy-ratio parameter, thermophoresis parameter and Brownian motion parameter, and a decreasing function of Lewis number. Nanoparticles volume fraction distribution is an increasing function of buoyancy-ratio parameter and thermophoresis parameter, and a decreasing function of Lewis number and Brownian motion parameter. Reduced Nusselt number and reduced skin friction number are increasing functions of nanoparticles volume fraction. In addition, a comparison between single phase model and double phase model has been shown for the first time. At certain values of key parameters, the same results for two models are obtained.

REFERENCES

1. Zhu, H., Y. Lin, and Y. Yin. A novel one-step chemical method for preparation of copper nanofluids // J. Colloid Interface Sci. 2004 – Vol. 277. – P. 100–103.
2. Eastman, J. A., S. U. S. Choi, S. Li, W. Yu, and L. J. Thomson. Anomalously increased effective thermal conductivities of ethylene glycol based nanofluids containing // Appl. Phys. Lett. 2001. – Vol. 78. – P. 718–720.
3. Choi, S. U. S., Z.G. Zhang, W. Yu, F.E. Lockwood, and E. A. Grulke. Anomalous thermal conductivity enhancement in nano-tube suspensions // Appl. Phys. Lett. 2001. – Vol. 79. – P. 2252–2254.
4. Hong T. K., H. S. Yang and C. J. Choi. Study of the enhanced thermal conductivity of Fe nanofluids // J. Appl. Phys. 2005. – Vol. 97: 064311
5. Chopkar, M, P. K. Das, and I. Manna. Synthesis and characterization of nanofluid for advanced heat transfer applications // Scr. Mater. 2006. – Vol. 55. – P. 549–552.
6. Das, S. K., N. Putra, P. Thiesen, and W. Roetzel. Temperature dependence of thermal conductivity enhancement for nanofluids // J. Heat Transfer. – 2003. – Vol. 125. – P. 567–574.
7. Chon, C. H., K. D., Kihm, S. P. Lee, and S. U. S. Choi. Empirical correlation finding the role of temperature and particle size for nanofluid (Al2O3) thermal conductivity enhancement // Appl. Phys. Lett. – 2005. – Vol. 87: 153107.
8. Ding, Y., and D. Wen. Particle migration in a flow of nanoparticle suspensions // Powder Technol. – 2005. – Vol. 149. – P. 84–92.
9. Xuan, Y., and Q. Li. Investigation on convective heat transfer and flow features of nanofluids // J. Heat Transfer. – 2003. – Vol. 125. – P. 151–155.
10. Putra, N., W. Roetzel, and S. K. Das. Natural convection of nano-fluids // Heat Mass Transfer. – 2003. – Vol. 39. – P. 775–784.

11. Wang, X., X. Xu, and S. U. S. Choi. Thermal conductivity of nanoparticle–fluid mixture // J. Thermophys. Heat Transfer. – 1999. – Vol. 13. – P. 474–480.
12. Xuan, Y., and Q. Li. Heat transfer enhancement of nanofluid // Int. J. Heat Fluid Flow. – 2000. – Vol. 21. – P. 58–64.
13. Keblinski, P., S. R. Phillpot, S. U. S. Choi, and J. A. Eastman. Mechanism of heat flow in suspensions of nano-sized particles (nanofluids) // Int. J. Heat and Mass Transfer. – 2002. – Vol. 45. – P. 855–863.
14. Yu, W., and S. U. S. Choi. The role of interfacial layers in the enhanced thermal conductivity of nanofluids: a renovated Hamilton–Crosser model // J. Nanopart Res. – 2004. – Vol. 6. – P. 355–361.
15. Xue, Q.-Z. Model for effective thermal conductivity of nanofluids // Phys. Lett. A. – 2003. – Vol. 307. – P. 313–317.
16. Xie, H. Q., J. C. Wang, T. G. Xi, and Y. Liu. Thermal conductivity of suspensions containing nanosized SiC particles // Int. J. Thermophys. – 2002. – Vol. 23. – P. 571–580.
17. Lee, D., J.-W. Kim, and B. G. Kim. A new parameter to control heat transport in nanofluids: surface charge state of the particle in suspension // J. Phys. Chem. B. – 2006. – Vol. 110. – P. 4323–4328.
18. Xuan, Y., and W. Roetzel. Conceptions for heat transfer correlation of nanofluids // Int. J. Heat Mass Transfer. – 2000. – Vol. 43. – P. 3701–3707.
19. Khaled, A. R. A., and K. Vafai . Heat transfer enhancement through control of thermal dispersion effects // Int. J. Heat and Mass Transfer. – 2005. – Vol. 48. – P. 2172–2185.
20. Buongiorno, J. Convective transport in nanofluids// J. Heat Transfer. – 2006. – Vol. 128. – P. 240–250.
21. Kim, J., Y. T., Kang, and C. K. Choi . Analysis of convective instability and heat transfer characteristics of nanofluids// Phys. Fluids. – 2004. – Vol. 16. – P. 2395–2401.

22. Jaluria Y. Natural Convection Heat and Mass Transfer. U.K: Pergamon Press; 1980.
23. Bejan A. Convection Heat Transfer. New York: Springer; 2013.
24. Shenoy A, Sheremet M, Pop I. Convective Flow and Heat Transfer from Wavy Surfaces: Viscous Fluids, Porous Media and Nanofluids. New York: CRC Press; 2016.
25. Burden L, Faires J.D. Numerical analysis. Boston: PWS Kent, 1986.
26. Trimbitas R.T. Numerical analysis in MATLAB. Cluj-Napoca: Cluj University Press, 2009.
27. .C. Crepeau, R. Clarksean Similarity solutions of natural convection with internal heat generation // J. Heat Transfer. – 1997. – Vol. 119. – P. 183–185.
28. A.V. Kuznetsov, D.A. Nield. Natural convective boundary-layer flow of a nanofluid past a vertical plate // International Journal of Thermal Sciences. – 2010. – Vol. 49. – P. 243–247.
29. W. Ibrahim, O.D. Makinde The effect of double stratification on boundary-layer flow and heat transfer of nanofluid over a vertical plate // Computer & Fluids. – 2013. – Vol. 86. – P. 433–441.
30. Saghir, M.Z., Ahadi, A., Mohamad, A., and Srinivasan, S. “Water aluminum oxide nanofluid benchmark model”// Int. J. Thermal Sciences. – 2016. – Vol. 109. – P. 148–158.
31. Ho, C.J., Liu, W.K., Chang, Y.S., and Lin, C.C. “Natural convection heat transfer of alumina-water nanofluid in vertical square enclosures: An experimental study”// Int. J. Thermal Sciences. – 2010. – Vol. 49. – P. 1345–1353.
32. Brinkman H.C. The viscosity of concentrated suspensions and solutions// Journal of Chemical Physics. – 1952. – Vol. 20. – P. 571–581.
33. Rana P., Bhargava R. Numerical study of heat transfer enhancement in mixed convection flow along a vertical plate with heat source/sink utilizing

nanofluids// Commun Nonlinear Sci Numer Simulat. – 2011. – Vol. 16. – P. 4318–4334.

APPENDIX

Runge Kutta method 4th order:

For example, a first-order differential equation is given by:

$$\frac{du(x)}{dx} = u'(x) = f(u(x), x)$$

Initial condition $u(x_0) = u_0$

We will find a solution for this problem in the interval: [0;1] (x_0=0)

First of all, we divide the interval (0,1) into N equal intervals: N *h= 1

In which, the number of small intervals: N = $\frac{1}{h}$

We will use the following approximations for the slopes in x_0:

$k_1 = f(u(x_0), x_0)$

$k_2 = f(u(x_0) + k_1 \frac{h}{2}, x_0 + \frac{h}{2})$

$k_3 = f(u(x_0) + k_2 \frac{h}{2}, x_0 + \frac{h}{2})$

$k_4 = f(u(x_0) + k_3 h, x_0 + h)$

Then we use the weighted sum of these slopes to get our estimate of u (x_0 + h) $u(x_0 + h) = u(x_0) + \frac{k_1 + 2k_2 + 2k_3 + k_4}{6} h$ = $u(x_0)$ + m*h

Continuing N times this step until x = 1, we obtain u (1)